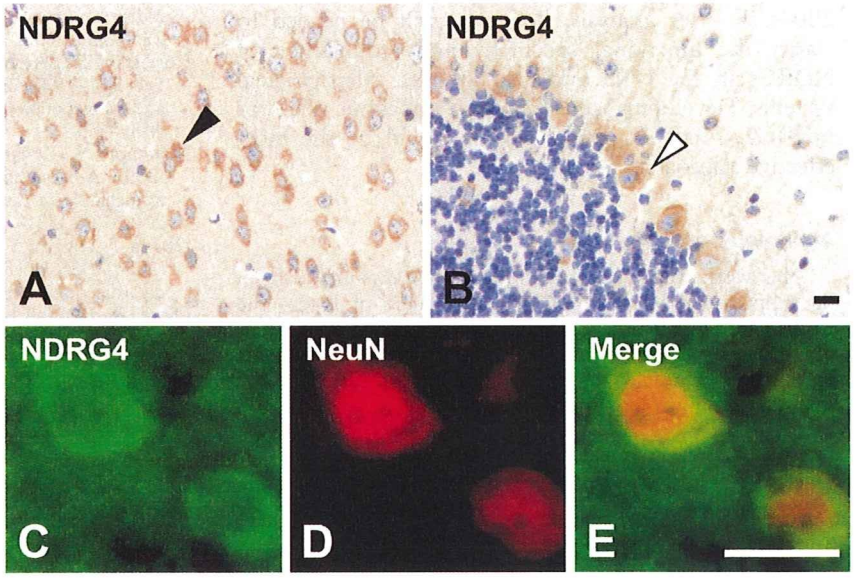

Figure 7 Localization of NDRG4 in the brain. NDRG4 was detected in most cells in the cerebrum, but especially strongly in the neurons (arrowhead in **A**) and Purkinje cells in the cerebellum (open arrowhead in **B**). Strong expression of NDRG4 (**C**) was colocalized with a neuron marker NeuN (**D**). Merged images are shown in **E**. Bar = 10 μm.

with NDRG2 and NDRG4. Immunohistochemical analysis, however, could fortunately discriminate NDRG1 from NDRG3: anti-NDRG1 showed a cytoplasmic staining pattern in particular cells, whereas anti-NDRG3 reacted with the nuclei in most cells of the brain.

We demonstrated here that NDRG1 was mainly localized in the oligodendrocytes (Figure 4). Another group (Wakisaka et al. 2003), however, has reported immunohistochemical data inconsistent with the present study. That report demonstrated that the localization of NDRG1 is changed from hippocampal neurons to astrocytes during postnatal development in the rat brain. Although the inconsistency may be caused by the difference in animal species or developmental process, the possibility of unexpected cross-reactions of their antibody to other NDRGs (probably NDRG2) cannot be ruled out. In fact, our observation of NDRG1 localization in oligodendrocytes is consistent with that of another report (Berger et al. 2004).

The oligodendrocyte is a glial cell engaged in the formation of myelin sheaths in the CNS, whereas the Schwann cell expressing NDRG1 plays an analogous role in the PNS. NDRG1, therefore, may contribute to cellular processes in the development or maintenance of myelin sheaths. Although the loss of NDRG1 in Schwann cells led to demyelination in the sciatic nerves (Okuda et al. 2004), the loss in oligodendrocytes had no effect in the brain (Figure 3). These observations suggested that other NDRGs may compensate for the NDRG1 deficiency in oligodendrocytes but cannot do so in Schwann cells. In fact, all NDRGs except NDRG1 were less expressed in the sciatic nerve than in the brain (Okuda et al. 2004).

NDRG2 was localized to the astrocytes in the cerebrum and to Bergmann glial cells in the cerebellum (Figure 5). NDRG3 was expressed in most cells in the cerebrum and cerebellum, and the subcellular localization of NDRG3 was restricted in the nucleus (Figure 6). These marked differences from NDRG1 in the cellular and subcellular localization suggested that NDRG2 and NDRG3 may not have a redundant function of NDRG1. In fact, NDRG2 and NDRG3 were unable to compensate for the NDRG1 deficiency in sciatic nerves despite their expression in the tissue (Okuda et al. 2004).

In contrast to NDRG2 and NDRG3, NDRG4 may be a likely candidate of compensators for the NDRG1 deficiency in the brain. NDRG4 was abundantly expressed in the brain, especially in the neurons and Purkinje cells (Figure 7), the latter of which were also rich in NDRG1. NDRG1 was originally identified as a gene upregulated with homocysteine treatment (Kokame et al. 1996), and expression of NDRG4 is also induced by homocysteine (Nishimoto et al. 2003). These similarities between NDRG1 and NDRG4 may signify their functional similarity. Failure in compensation for the loss of NDRG1 in the *Ndrg1*-deficient PNS can be explained by the fact that there is little expression of NDRG4 in the sciatic nerves (Okuda et al.

Table 1 Summary of major expression cells of NDRG family proteins in the brain

	NDRG1	NDRG2	NDRG3	NDRG4
Cerebrum	Oligodendrocytes Ependymal cells	Astrocytes	Most cells (nucleus)	Most cells
Cerebellum	Purkinje cells	Bergmann glia	Purkinje cells (nucleus) Most cells (nucleus)	Purkinje cells

The Journal of Histochemistry & Cytochemistry

2004). Further analysis, however, will be needed to clarify the functional specificity and redundancy of NDRGs in the CNS and also in other physiological systems. Developing and analyzing knockout mice for NDRG2, NDRG3, and NDRG4 would be the most effective approach.

Acknowledgments

This work was supported in part by Grants-in-Aid from the Ministry of Health, Labor, and Welfare of Japan; the Ministry of Education, Culture, Sports, Science, and Technology of Japan; and the Program for the Promotion of Fundamental Studies in Health Sciences of the National Institute of Biomedical Innovation (NIBIO).

Literature Cited

Agarwala KL, Kokame K, Kato H, Miyata T (2000) Phosphorylation of RTP, an ER stress-responsive cytoplasmic protein. Biochem Biophys Res Commun 272:641–647

Bandyopadhyay S, Pai SK, Gross SC, Hirota S, Hosobe S, Miura K, Saito K, et al. (2003) The Drg-1 gene suppresses tumor metastasis in prostate cancer. Cancer Res 63:1731–1736

Berger P, Sirkowski EE, Scherer SS, Suter U (2004) Expression analysis of the N-Myc downstream-regulated gene 1 indicates that myelinating Schwann cells are the primary disease target in hereditary motor and sensory neuropathy-Lom. Neurobiol Dis 17:290–299

Guan RJ, Ford HL, Fu Y, Li Y, Shaw LM, Pardee AB (2000) Drg-1 as a differentiation-related, putative metastatic suppressor gene in human colon cancer. Cancer Res 60:749–755

Kalaydjieva L, Gresham D, Gooding R, Heather L, Baas F, de Jonge R, Blechschmidt K, et al. (2000) N-myc downstream-regulated gene 1 is mutated in hereditary motor and sensory neuropathy-Lom. Am J Hum Genet 67:47–58

Kalaydjieva L, Hallmayer J, Chandler D, Savov A, Nikolova A, Angelicheva D, King RH, et al. (1996) Gene mapping in Gypsies identifies a novel demyelinating neuropathy on chromosome 8q24. Nat Genet 14:214–217

Kokame K, Kato H, Miyata T (1996) Homocysteine-respondent genes in vascular endothelial cells identified by differential display analysis. GRP78/BiP and novel genes. J Biol Chem 271: 29659–29665

Kovacevic Z, Richardson DR (2006) The metastasis suppressor, Ndrg-1: a new ally in the fight against cancer. Carcinogenesis 27: 2355–2366

Kurdistani SK, Arizti P, Reimer CL, Sugrue MM, Aaronson SA, Lee SW (1998) Inhibition of tumor cell growth by RTP/rit42 and its responsiveness to p53 and DNA damage. Cancer Res 58: 4439–4444

Nishimoto S, Tawara J, Toyoda H, Kitamura K, Komurasaki T (2003) A novel homocysteine-responsive gene, smap8, modulates mitogenesis in rat vascular smooth muscle cells. Eur J Biochem 270:2521–2531

Okuda T, Higashi Y, Kokame K, Tanaka C, Kondoh H, Miyata T (2004) Ndrg1-deficient mice exhibit a progressive demyelinating disorder of peripheral nerves. Mol Cell Biol 24:3949–3956

Okuda T, Kondoh H (1999) Identification of new genes Ndr2 and Ndr3 which are related to Ndr1/RTP/Drg1 but show distinct tissue specificity and response to N-myc. Biochem Biophys Res Commun 266:208–215

Piquemal D, Joulia D, Balaguer P, Basset A, Marti J, Commes T (1999) Differential expression of the RTP/Drg1/Ndr1 gene product in proliferating and growth arrested cells. Biochim Biophys Acta 1450:364–373

Qu X, Zhai Y, Wei H, Zhang C, Xing G, Yu Y, He F (2002) Characterization and expression of three novel differentiation-related genes belong to the human NDRG gene family. Mol Cell Biochem 229:35–44

Shimono A, Okuda T, Kondoh H (1999) N-myc-dependent repression of *Ndr1*, a gene identified by direct subtraction of whole mouse embryo cDNAs between wild type and *N-myc* mutant. Mech Dev 83:39–52

Stein S, Thomas EK, Herzog B, Westfall MD, Rocheleau JV, Jackson RS 2nd, Wang M, et al. (2004) NDRG1 is necessary for p53-dependent apoptosis. J Biol Chem 279:48930–48940

van Belzen N, Dinjens WN, Diesveld MP, Groen NA, van der Made AC, Nozawa Y, Vlietstra R, et al. (1997) A novel gene which is up-regulated during colon epithelial cell differentiation and down-regulated in colorectal neoplasms. Lab Invest 77:85–92

Wakisaka Y, Furuta A, Masuda K, Morikawa W, Kuwano M, Iwaki T (2003) Cellular distribution of NDRG1 protein in the rat kidney and brain during normal postnatal development. J Histochem Cytochem 51:1515–1525

Xu B, Lin L, Rote NS (1999) Identification of a stress-induced protein during human trophoblast differentiation by differential display analysis. Biol Reprod 61:681–686

Zhou D, Salnikow K, Costa M (1998) *Cap43*, a novel gene specifically induced by Ni^{2+} compounds. Cancer Res 58:2182–2189

Zhou RH, Kokame K, Tsukamoto Y, Yutani C, Kato H, Miyata T (2001) Characterization of the human NDRG gene family: a newly identified member, NDRG4, is specifically expressed in brain and heart. Genomics 73:86–97

Available online at www.sciencedirect.com
ScienceDirect
Biochemical and Biophysical Research Communications 367 (2008) 616–622
BBRC
www.elsevier.com/locate/ybbrc

Enhanced autophagy and mitochondrial aberrations in murine G_{M1}-gangliosidosis

Ayumi Takamura [a,b], Katsumi Higaki [a,*], Kenya Kajimaki [a,c], Susumu Otsuka [a,d], Haruaki Ninomiya [e], Junichiro Matsuda [f], Kousaku Ohno [g], Yoshiyuki Suzuki [h], Eiji Nanba [a]

[a] *Division of Functional Genomics, Research Center for Bioscience and Technology, Tottori University, 86 Nishi-machi, Yonago 683-8503, Japan*
[b] *Department of Biosignaling, School of Life Sciences, Tottori University, 86 Nishi-machi, Yonago 683-8503, Japan*
[c] *Department of Molecular and Cellular Biology, School of Life Sciences, Tottori University, 86 Nishi-machi, Yonago 683-8503, Japan*
[d] *Department of Biomedical Science, Institute of Regenerative Medicine and Biofunction, Graduate School of Medical Science, Tottori University, 86 Nishi-machi, Yonago 683-8503, Japan*
[e] *Department of Biological Regulation, School of Health Science, Faculty of Medicine, Tottori University, 86 Nishi-machi, Yonago 683-8503, Japan*
[f] *National Institute of Biomedical Innovation, 7-6-8 Saito-asagi, Ibaraki, 567-0085, Japan*
[g] *Division of Child Neurology, Tottori University Faculty of Medicine, 36-1 Nishi-machi, Yonago 683-8504, Japan*
[h] *Graduate School, International University of Health and Welfare, 2600-1 Kita-Kanemaru, Otawara 324-8501, Japan*

Received 28 December 2007
Available online 9 January 2008

Abstract

G_{M1}-gangliosidosis is an autosomal recessive lysosomal lipid storage disorder, caused by mutations of the lysosomal β-galactosidase (β-gal) and results in the accumulation of G_{M1}. The underlying mechanisms of neurodegeneration are poorly understood. Here we demonstrate increased autophagy in β-gal-deficient (β-gal$^{-/-}$) mouse brains as evidenced by elevation of LC3-II and beclin-1 levels. Activation of autophagy in the β-gal$^{-/-}$ brain was found to be accompanied with enhanced Akt–mTOR and Erk signaling. In addition, the mitochondrial cytochrome *c* oxidase activity was significantly decreased in brains and cultured astrocytes from β-gal$^{-/-}$ mouse. Mitochondria isolated from β-gal$^{-/-}$ astrocytes were morphologically abnormal and had a decreased membrane potential. These cells were more sensitive to oxidative stress than wild type cells and this sensitivity was suppressed by ATP, an autophagy inhibitor 3-methyladenine and a pan-caspase inhibitor z-VAD-fmk. These results suggest activation of autophagy leading to mitochondrial dysfunction in the brain of G_{M1}-gangliosidosis.

Keywords: G_{M1}-gangliosidosis; Lysosome; Autophagy; mTOR; Mitochondria; Astrocyte; Neurodegeneration

G_{M1}-gangliosidosis (OMIM 230500) is an autosomal recessive lysosomal lipid storage disorder with progressive central nervous system dysfunction, visceromegaly, and skeletal dysplasias. It is caused by deficiency of lysosomal acid β-galactosidase (β-gal) due to mutations in the *GLB1* gene [1]. Three clinical forms (infantile, juvenile, and adult/chronic) have been distinguished according to the age of onset and severity, mainly due to different residual activities of the mutant enzymes and hence different levels of the substrate accumulation in tissues, especially in the brain. Pathologically, typical lamellar inclusions or membranous cytoplasmic bodies are found in neurons of human, mouse, and other animal models of G_{M1}-gangliosidosis [2–4]. Neurons are the primary target of storage, but astrocytes may also appear abnormally vacuolated [5]. Recently, we have developed chemical chaperone therapy for brain pathology in G_{M1}-gangliosidosis [6,7]. However,

Abbreviations: LC3, microtubule-associated protein 1 light chain 3; mTOR, mammalian target of rapamycin; PI3K, phosphatidylinositol 3 kinase; LDH, lactate dehydrogenase; 3-MA, 3-methyladenine; DMEM, Dulbecco's modified Eagle's medium; PBS, phosphate-buffered saline; BSA, bovine serum albumin.

* Corresponding author. Fax: +81 859 38 6470.
E-mail address: kh4060@grape.med.tottori-u.ac.jp (K. Higaki).

0006-291X/$ - see front matter © 2008 Elsevier Inc. All rights reserved.
doi:10.1016/j.bbrc.2007.12.187

underlying biological mechanisms responsible for neurodegeneration still remain uncertain [8].

Macroautophagy (hereafter referred to as autophagy) involves bulk degradation of complete regions of the cytosol [9]. The target regions are initially sequestered in multimembrane vacuoles, known as autophagosome which eventually fused with lysosomes for degradation. Autophagy plays a cytoprotective role in low-nutrient conditions and disease states by catabolizing intracellular substrates for energy supply and by removing failing mitochondria and other factors that trigger cell death [10]. Dysfunction of autophagy can disrupt neuronal function and ultimately lead to neurodegeneration [11].

In this study, we demonstrate enhanced autophagy and mitochondrial alterations in the G_{M1}-gangliosidosis mouse brain, which might lead to neurodegeneration in this disease.

Materials and methods

Antibodies and reagents. Monoclonal anti-G_{M1} (GMB16) was from Seikagaku Corp. (Tokyo, Japan), polyclonal anti-LC3 (PD014) was from MBL International Corp. (Woborn, MA, USA), polyclonal anti-beclin-1 (H-300) was from Santa Cruz Biotechnology Inc. (Santa Cruz, CA, USA) and polyclonal anti-Atk, anti-phospho-Akt (Ser473), anti-mTOR, anti-phospho-mTOR (Ser2448), anti-S6 ribosomal protein (5G10), and anti-phospho-S6 ribosomal protein (Ser235/236) were from Cell Signaling Technology (Boston, MA, USA). Paraquat, ATP and chloroquine were purchased from Wako (Tokyo, Japan), 3-methyladenine (3-MA), and rapamycin were from Sigma (St. Louis, MO, USA) and z-VAD-fmk was from Promega (Madison, WI, USA).

Mice and tissue collection. A C57BL/6-based congenic mouse strain with β-gal-deficiency (β-gal$^{-/-}$) was established as reported previously [3,6]. All animal procedures were carried out following the protocols approved by the committee for animal experiments in Tottori University and β-gal$^{-/-}$ mice was obtained by cross bleeding. For tissue staining, mice were anesthesized and perfused with 4% paraformaldehyde (PFA) in sodium phosphate, pH 7.4. Brains were embedded in OTC compound (Sakura Finetechnical Co., Tokyo, Japan) and 8 μm sections were cut using a cryostat. For protein extractions, tissues were removed and frozen in liquid nitrogen.

Primary culture of astrocytes. For astrocyte preparation, brains from postnatal day four mice were removed under anesthesia. The cerebral cortex was dissociated and cells were seeded on plastic dishes in DMEM-F12 supplemented with 15% fetal bovine serum (FBS). They were cultured for 7 days, trypsinized, and seeded on dishes with DMEM-F12 with 10% FBS. They were confirmed to be GFAP-positive astrocytes at 3 weeks by immunostaining with polyclonal anti-GFAP (data not shown). Lactate dehydrogenase (LDH) cytotoxicity assay (Wako, Tokyo, Japan) was performed following the manufacturer's instruction.

Immunoblot analysis. Mouse brains were lysed by sonication in a buffer containing 10 mM Tris–HCl (pH 7.4), 150 mM NaCl, 1 mM EDTA, 1 mM EGTA plus protease inhibitor cocktail (Roche). Protein was quantified using Color-Producing Solution (Wako). Samples were separated on 10% SDS–PAGE and transferred on a nylon membrane (Millipore) using a semi-dry transfer blotter (BioRad). Membranes were incubated in a polyclonal antibody followed by a horseradish peroxidase-linked donkey anti-rabbit IgG antibody (Amersham). Detection was performed using ECL (Amersham Pharmacia Biotech) and images were captured in X-ray film or a LAS-1000 plus imager (Fujifilm).

Immunofluorescence staining. Brain sections were permiabilized with 0.25% Triton X-100 in PBS for 15 min at room temperature, blocked with 1% BSA in PBS for 1 h at room temperature, and incubated with the first antibody at 4 °C overnight. Bind antibodies were detected with Alexafluor-conjugated secondary antibody for 1 h at room temperature. Fluorescence images were obtained using confocal microscopy (Leica, TCS-SP2; Wetzler, Germany).

Mitochondrial assay. Mitochondria were isolated from the mouse brain and cultured astrocytes using mitochondrial isolation kit (BioChain Ins. Hayward, CA, USA) and the enzyme activity of cytochrome *c* oxidase was determined using mitochondrial activity kit (BioChain Ins.) following the manufacturer's instruction. For mitochondrial labeling, cultured astrocytes were seeded on sterile cover slips or glass base dishes (Iwaki, Tokyo, Japan) and incubated in Hanks' balanced salt solution containing 100 nM MitoTracker Red CMXRos or 3 μM Mitotracker JC-1 (MolecularProbes Inc., Eugene, OR, USA) for 20 min at 37 °C. Cells were then washed with Hanks' balanced salt solution and fluorescent images were obtained using confocal microscopy.

Results

G_{M1} accumulation and sequestration of autophagosomes proteins in the β-gal$^{-/-}$ mice brain

Microtubule-associated protein 1 light chain 3 (LC3), a mammalian homolog of the yeast autophagic protein Atg8, has been used as an autophagosomal marker [9]. Cleavage of LC3 in its carboxy terminal gives rise to a cytosolic soluble form LC3-I which is further modified into LC3-II, a protein that associate with autophagosomes. Brain levels of LC3 were assessed by immunoblotting. Although levels of LC3-I and LC3-II in β-gal$^{-/-}$ mice did not significantly differ from those in wild type (WT) mice at 10-day-old, the level of LC3-II were significantly higher in mutant mice at 10 months of age (Fig. 1A). G_{M1} and LC3 double immunofluorescence showed co-localization of LC3-immunopositive-granules with G_{M1} in neurons of β-gal$^{-/-}$ mice at 10 months (Fig. 1B). Beclin-1 is the mammalian ortholog of yeast Atg6, and is a part of the Class III phosphatidylinositol 3 kinase (PI3K) complex that participate in autophagosome formation [9]. The level of beclin-1 was increased in brain lysates from 10-month-old β-gal$^{-/-}$ mice when compared to WT mice (Fig. 1C and D). The Akt/mammalian target of rapamycin (mTOR) and the extracellular signal kinase (Erk) are two major pathways that regulate autophagy [10,12]. Phsphorylation of Akt, Erk, and mTOR were increased, whereas no obvious alteration of S6 was detected in the brain lysates of β-gal$^{-/-}$ mice at 10 months (Fig. 2A and B).

Mitochondrial alterations in β-gal$^{-/-}$ mice

Autophagy is a highly regulated process that is involved in the turnover of long-lived proteins and whole organelles. It can specifically target distinct organelles, such as mitochondria in mitopathy and the endoplasmic reticulam in reticulopathy [9]. We next sought to examine whether sequestration in autophagic vacuoles affects mitochondrial function in this mouse model. The level of mitochondrial cytochrome *c* oxidase activity was significantly decreased in the brain of β-gal$^{-/-}$ mice than that of WT mice at 10 months (Fig. 3A). Similarly, cultured astrocytes from

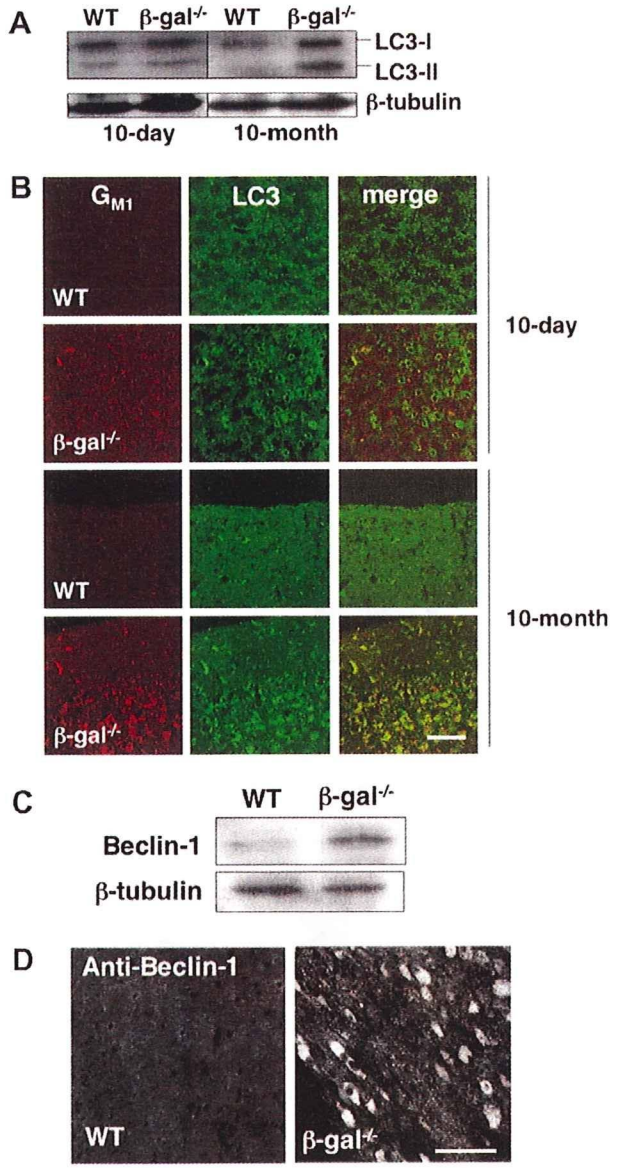

Fig. 1. Elevation of LC3-II and beclin-1 expression in β-gal$^{-/-}$ mouse brain. Cerebellar lysates from WT and β-gal$^{-/-}$ mice were subjected to Western blotting with anti-LC3 (A) or anti-beclin-1 (C). Immunofluorescence of cellular distribution of LC3 (B) and beclin-1 (D) proteins in the frontal cerebral cortex of WT and β-gal$^{-/-}$ mice. Scale bar = 80 μm.

β-gal$^{-/-}$ mice showed lysosomal accumulation of G_{M1} and elevated LC3-II and beclin-1 levels (data not shown), and it had a decreased cytochrome *c* oxidase activity (Fig. 3A). Next, the morphology and the membrane potential of mitochondria were examined in cultured astrocytes using confocal microscopy. There were obvious differences in mitochondrial morphology between WT and β-gal$^{-/-}$ astrocytes. In WT astrocytes, mitochondria were organized as extended tubular structures, whereas β-gal$^{-/-}$ astrocytes contained smaller, fragmented or circulated mitochondria (Fig. 3B and C). When cells were stained with Mitotracker JC-1, a marker of the mitochondrial membrane potential,

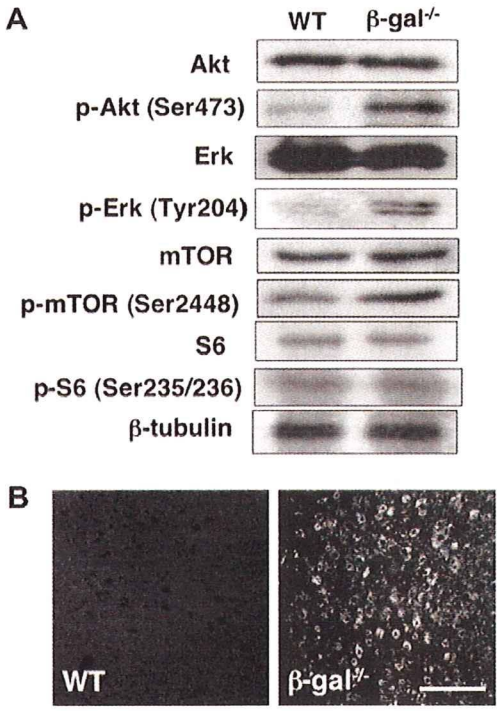

Fig. 2. Changes in Akt/mTOR and Erk signals in β-gal$^{-/-}$ mouse brain. (A) Cerebellar lysates from postnatal of 10-month-old WT and β-gal$^{-/-}$ mice were subjected to Western blotting with indicated antibodies. (B) Cellular distribution of p-mTOR (Ser2448) in the frontal cerebral cortex of WT and β-gal$^{-/-}$ mice at 10 months of age. Scale bar = 80 μm.

the intensity of red and green fluorescence was decreased in β-gal$^{-/-}$ astrocytes compared to the WT (Fig. 3D).

Dysfunction of autophagic-lysosomal pathways and mitochondria

To examine functional relevance of mitochondrial dysfunction to cell death, we treated cultured astrocytes with oxidative stress reagent paraquat. LDH release assay revealed a significant increase of the percentage of dead cells was noted in β-gal$^{-/-}$ astrocytes compared to that in WT cells (Fig. 4A). We also attempted to characterize the impairment in autophagy and mitochondria in β-gal$^{-/-}$ astrocytes. LDH release in paraquat (250 μM)-treated-β-gal$^{-/-}$ astrocytes was significantly suppressed by addition of 0.5 mM ATP in the medium for 24 h (Fig. 4B). We next examined effects of 3-MA and rapamycin, which inhibit or induce autophagy, respectively [13], 3-MA at 10 mM reduced paraquat-induced-LDH release in β-gal$^{-/-}$ astrocytes, whereas, rapamycin (2 μg/ml) had no effects on cell death. We also examined a cell-permeable pan-caspase inhibitor, z-VAD-fmk, since autophagic cell death was partly mediated by caspase activation [10]. z-VAD-fmk (100 μM) significantly decreased cell death in paraquat-treated-β-gal$^{-/-}$ astrocytes. Under these conditions, none of the drugs affected LDH release in

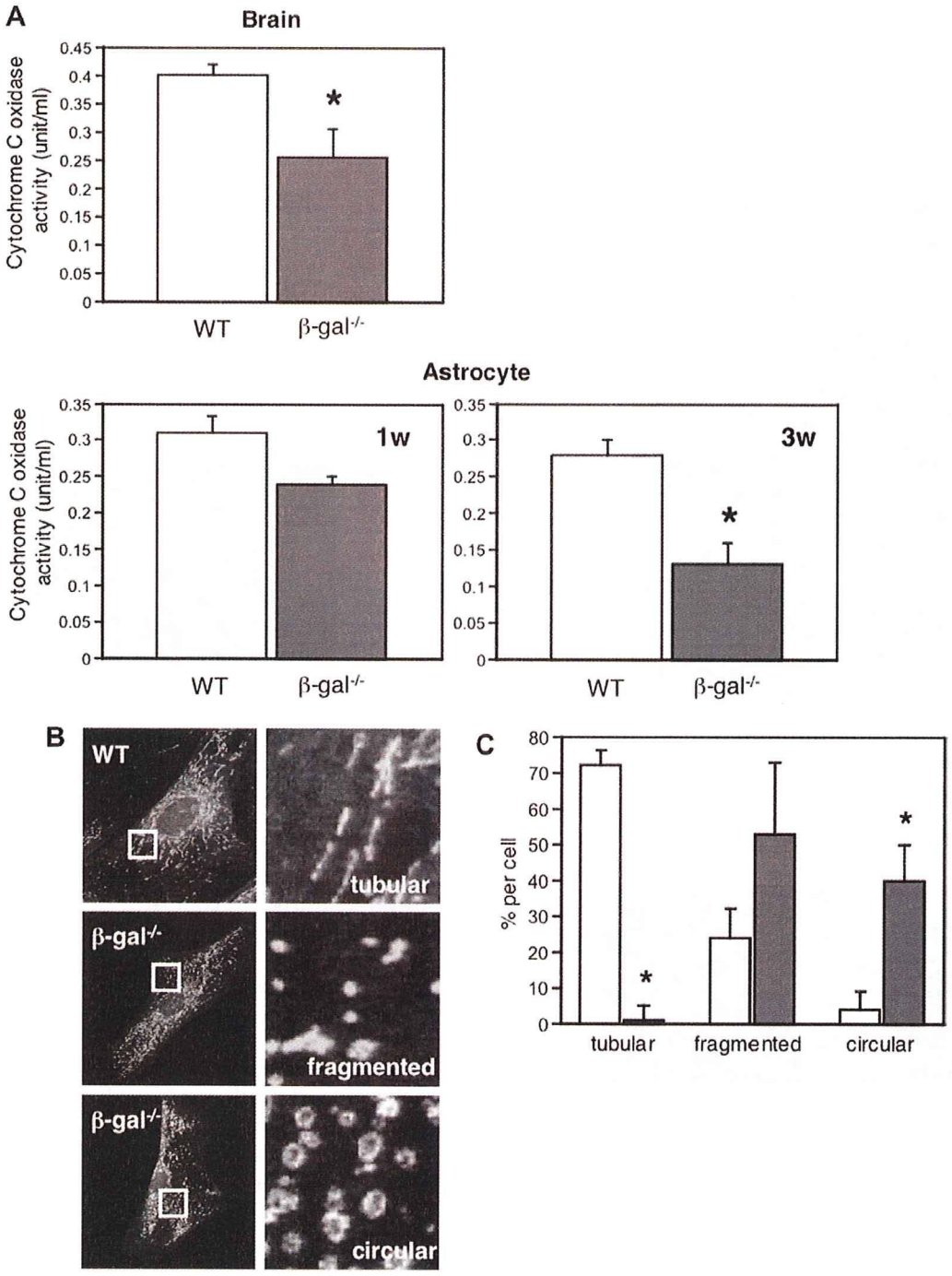

Fig. 3. Mitochondrial alteration in β-gal$^{-/-}$ mouse brain and astrocyte. (A) Levels of cytochrome *c* oxidase activities in extracts from the brain and primary astrocytes of WT and β-gal$^{-/-}$ mice. Values are means ± SEM from three independent experiments, $^{*}p < 0.01$ significantly differ from the value of WT cells. (B) Primary astrocytes from neonatal WT and β-gal$^{-/-}$ cortex were cultured for 3 weeks and labeled with MitoTracker Red. Morphological analysis of mitochondria was obtained using confocal microscopy. (C) The number of cells with each morphology of mitochondria was computed. Values for the percent of total cell number from three independent experiments. $n = 30$ cells and values are means ± SEM. (open bars: WT; dark bars: β-gal$^{-/-}$) (D) Primary-cultured astrocytes were labeled with JC-1. Shown are the representative images obtained by confocal microscopy using red and green channels. Scale bar = 25 μm. (For interpretation of the references to color in this figure legend, the reader is referred to the web version of this paper.)

WT astrocytes. Chloroquine, an inhibitor of autophagosome–lysosome fusion, induced cell death in WT astrocytes after treatment with paraquat, and this cell death was suppressed by ATP, 3-MA and z-VAD-fmk (Fig. 4B).

Discussion

One of the most important functions of autophagy is to maintain cellular energy subjected to nutrient deprivation

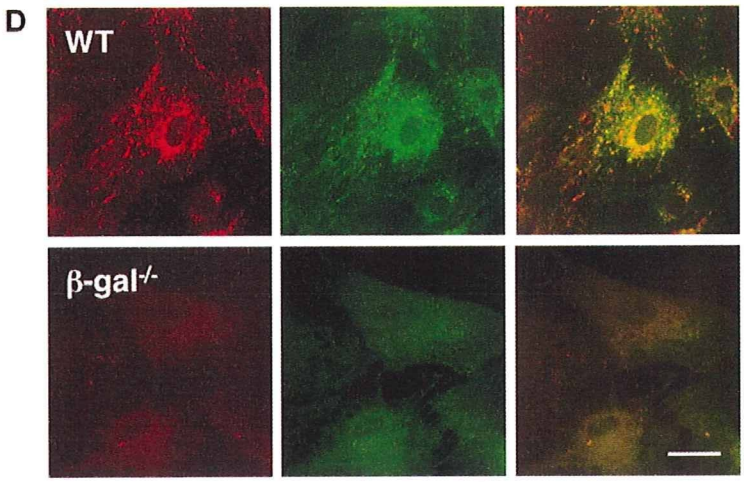

Fig. 3 (*continued*)

and potentially other forms of stress. Autophagy is a highly regulated process that is involved in the turnover of long-lived proteins and cytoplasmic constituents including mitochondria, endoplasmic reticulum, and ribosomes [10]. Molecular mechanisms that regulated autophagy in yeast and mammalian have recently been identified [9]. Knockout of autophagy genes causes abnormal accumulation in ubiquitinated inclusions and neurodegeneration in mice and that implicates in mechanisms of neurodegeneration [14,15].

In the present study, we showed increased levels of autophagic proteins in the β-gal$^{-/-}$ mice brain. Immunoblot analysis revealed an increase in levels of LC3-II, a widely used marker for autophagy, in all brain areas examined at 10 months of age. Levels were particularly high in cerebellum and brain stem, where severe neuronal death occurs in the β-gal-deficient human and mouse brain [1,3,4]. Increased autophagic stress was further confirmed by the presence of LC3-positive structures in cells with intracellular G_{M1} accumulations. This induction of autophagy was associated with increased expression of beclin-1. Beclin-1 is the mammalian ortholog of yeast Atg6, and is a part of the Class III PI3K machinery that participates in autophagosome formation [9].

Enhanced autophagy was recently reported in human skin fibroblasts and mice models of other types of lysosomal storage diseases, such as Danon disease [16], neuronal ceroid lipofuscinosis 2 [17], Pompe disease [18], mucolipidosis type IV [19] multiple sulfatase deficiency, mucopolysaccharidosis type IIA [20]. Induction of autophagy was also observed in the Niemann-Pick C1 (NPC1) mouse brain, which contained increased levels of beclin-1 [21].

The Akt–mTOR and Erk signaling pathways were also activated in β-gal$^{-/-}$ mice. Insulin signaling stimulates phosphorylation and activity of mTOR via Akt/PBK pathway and thereby represses autophagy in response to insulin-like and other growth factor signals [9]. Activation of these pathways is known to induce autophagy, although detailed mechanisms are still unknown. [12]. Previous studies have demonstrated localization of the active form of Erk in autophagosomes and mitochondria in degenerating brain [22], and that might happen in β-gal$^{-/-}$ brain.

Decrease in the cytochrome *c* oxidase activity, the morphological abnormality and high sensitivity to oxidative stress in the β-gal$^{-/-}$ astrocytes suggest mitochondrial abbreviations in this mouse. Inefficient autophagic-lysosomal fusion may cause accumulation of fragmented mitochondria. It is also possible that enhanced autophagy disrupted mitochondrial function. We showed that oxidative stress-induced cell death was suppressed by ATP, an autophagy inhibitor and a pan-caspase inhibitor in β-gal$^{-/-}$ astrocytes as well as in chloroquine-treated WT astrocytes, supporting the idea that enhanced autophagy induces mitochondrial dysfunction that leads to cell death. Mechanisms leading to cell death in astrocytes remain unclear, since functional relationship between autophagic cell death (also known as type II cell death) and apoptotic cell death (or type I cell death) is complex [10]. Autophagy and apoptosis may be triggered by common signals.

Autophagy has emerged as the major pathway involved in a number of neurodegenerative diseases, including Alzheimer disease [23], Parkinson disease [24], Huntington disease [25], and lysosomal storage diseases [16–21]. In each case, autophagic vacuoles accumulate in the affected neurons, indicating that activation of autophagy is a common feature of these diseases. However, the precise mechanisms leading to activation of autophagy remain elusive. Further investigation is warranted to clarify the mechanisms of enhanced autophagy in these disorders.

In summary, we provided evidence for abnormal activation of autophagy accompanied with mitochondrial alterations in the murine model of G_{M1}-gangliosidosis. Modulation of activity of autophagy and restoring mitochondrial functions may be of therapeutic benefit for this disease.

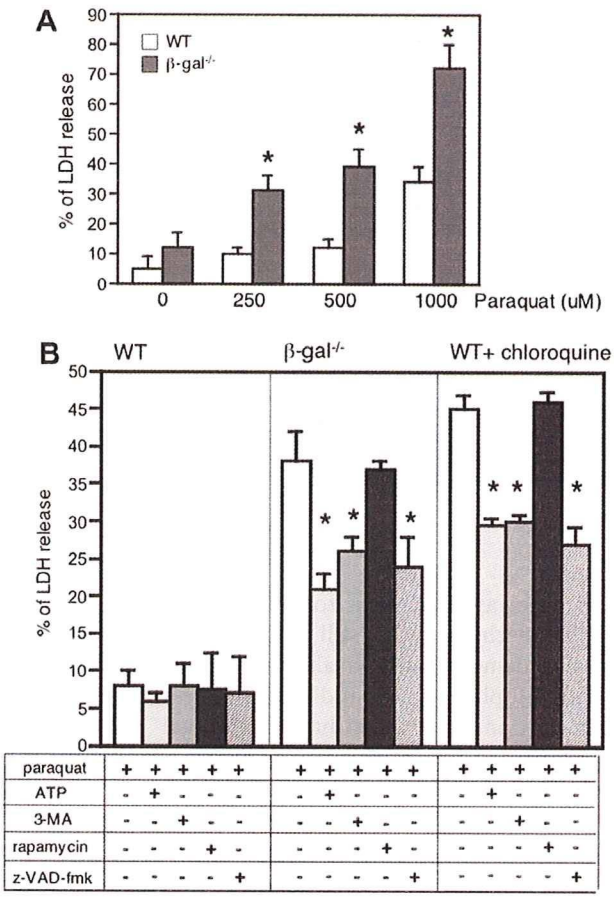

Fig. 4. Effects of ATP, 3-MA, rapamycin and a pan-caspase inhibitor on oxidative stress-induced cell death of astrocyte. (A) Lactate dehydrogenase (LDH) release assay. Astrocytes were cultured with or without paraquat for 24 h and the medium was collected for LDH release assay. Values were expressed as relative to the values from cells treated with 1% Tween 20. Each bar represents the mean (SEM) from three independent experiments. $^{*}p < 0.01$ significantly differ from the value of WT cells. (B) Both WT, β-gal$^{-/-}$ and chloroquine-treated WT astrocytes were treated with indicated drugs. LDH release assay were performed after 24 h treatment. Each bar represents the mean (SEM) from three independent experiments. $^{*}p < 0.01$ significantly differ from the value of paraquat-treated cells.

Acknowledgments

This work was supported by grants from Ministry of Education, Culture, Science, Sports, and Technology of Japan (13680918, 14207106, 16300141, 18390279, and 18790719) and Ministry of Health, Labour and Welfare of Japan (H10-No-006, H14-Kokoro-017, and H17-Kokoro-019).

References

[1] A. Oshima, E. Nanba, J. Matsuda, Y. Suzuki, β-Galactosidase deficiency (β-galactosidosis): GM1-gangliosidosis and Morquio B disease. In: D. Valle, A.L. Baudet, B. Vogelstein, et al., (Eds.), The Online Metabolic and Molecular Bases of Inherited Disease. 8th ed. McGraw-Hill, New York, 2007, Available from. <http://www.ommbid.com>.

[2] K. Suzuki, G.C. Chen, Morphological, histological and biochemical studies on a case of systemic late infantile lipidosis (generalized gangliosidosis), J. Neuropathol. Exp. Neurol. 27 (1968) 15–38.

[3] J. Matsuda, O. Suzuki, A. Oshima, A. Ogura, Y. Noguchi, Y. Yamamoto, T. Asano, K. Takimoto, K. Sukegawa, Y. Suzuki, M. Naiki, β-Galactosidase-deficient mouse as an animal model for G_{M1}-gangliosidosis, Glycoconj. J. 14 (1997) 729–736.

[4] C.N. Hahn, M. Martin, M. Schröder, M.T. Vanier, Y. Hara, K. Suzuki, K. Suzuki, A. d'Azzo, Generalized CNS disease and massive G_{M1}-ganglioside accumulation in mice defective in lysosomal acid β-galactosidase, Hum. Mol. Genet. 6 (1997) 205–211.

[5] J.E. Goldman, D. Katz, I. Rapin, D.P. Purpura, K. Suzuki, Chronic GM1 gangliosidosis presenting as dystonia: I. Clinical and pathological features, Ann. Neurol. 9 (1981) 465–475.

[6] J. Matsuda, O. Suzuki, A. Oshima, Y. Yamamoto, A. Noguchi, K. Takimoto, M. Itoh, Y. Matsuzaki, Y. Yasuda, S. Ogawa, Y. Sakata, E. Nanba, K. Higaki, Y. Ogawa, L. Tomonaga, K. Ohno, H. Iwasaki, H. Watanabe, R.O. Brady, Y. Suzuki, Chemical chaperone therapy for brain pathology in G_{M1}-gangliosidosis, Proc. Natl. Acad. Sci. USA 100 (2003) 15912–15917.

[7] Y. Suzuki, S. Ichinomiya, M. Kurosawa, M. Ohkubo, H. Watanabe, H. Iwasaki, J. Matsuda, Y. Noguchi, K. Takimoto, M. Itoh, M. Tabe, M. Iida, T. Kubo, S. Ogawa, E. Nanba, K. Higaki, K. Ohno, R.O. Brady, Chemical chaperone therapy: clinical effect in murine G_{M1}-gangliosidosis, Ann. Neurol. 62 (2007) 671–675.

[8] M. Jeyakumar, R.A. Dwek, T.D. Butters, F.M. Platt, Storage solutions: treating lysosomal disorders of the brain, Nat. Rev. Neurosci. 6 (2005) 1–12.

[9] M.C. Maiuri, E. Zalckvar, A. Kimchi, G. Kroemer, Self-eating and self-killing: crosstalk between autophagy and apoptosis, Nat. Rev. Mol. Cell Biol. 8 (2007) 741–752.

[10] B. Levine, J. Yuan, Autophagy in cell death: an innocent convict? J. Clin. Invest. 115 (2005) 2679–2688.

[11] M. Martinez-Vicente, A.M. Cuervo, Autophagy and neurodegeneration: when the cleaning crew goes on strike, Lancet Neurol. 6 (2007) 352–361.

[12] E. Corcelle, M. Nebout, S. Bekri, N. Gauthier, P. Hofman, P. Poujeol, P. Fenichel, B. Mograbi, Disruption of autophagy at the maturation step by the carcinogen lindane is associated with the sustained mitogen-activated protein kinase/extracellular signal-regulated kinase activity, Cancer Res. 66 (2007) 6861–6870.

[13] R.C. Paraguison, K. Higaki, K. Yamamoto, H. Matsumoto, T. Sasaki, N. Kato, E. Nanba, Enhanced autophagic cell death in expanded polyhistidine variants of HOXA1 reduces PBX1-coupled transcriptional activity and inhibits neuronal differentiation, J. Neuroci. Res. 85 (2007) 479–487.

[14] M. Komatsu, S. Waguri, T. Chiba, S. Murata, J. Iwata, I. Tanida, T. Ueno, M. Koike, Y. Uchiyama, E. Kominami, K. Tanaka, Loss of autophagy in the central nervous system causes neurodegeneration in mice, Nature 441 (2007) 880–884.

[15] T. Hara, K. Nakamura, M. Matsui, A. Yamamoto, Y. Nakahara, R. Suzuki-Migishima, M. Yokoyama, K. Mishima, I. Saito, H. Okano, N. Mizushima, Suppression of basal autophagy in neural cells causes neurogenerative disease mice, Nature 441 (2007) 885–889.

[16] Y. Tanaka, G. Guhde, A. Suter, E.L. Eskelinen, D. Hartmann, R. Lullmann-Rauch, P.M. Janssen, J. Blanz, K. von Figura, P. Saftig, Accumulation of autophagic vacuoles and cardiomyopathy in LAMP-2-deficient mice, Nature 406 (2000) 902–906.

[17] M. Koike, M. Shibata, S. Waguri, K. Yoshimura, I. Tanida, E. Kominami, T. Gotow, C. Peters, K. von Figura, N. Mizushima, P. Saftig, Y. Uchiyama, Participation of autophagy in storage of lysosomes in neurons from mouse models of neuronal ceroid-lipofuscinoses (Batten disease), Am. J. Pathol. 167 (2005) 1713–1728.

[18] T. Fukuda, L. Ewan, M. Bauer, R.J. Mattaliano, K. Zaal, E. Ralston, P.H. Plotz, N. Raben, Dysfunction of endocytic and autophagic pathways in a lysosomal storage disease, Ann. Neurol. 59 (2006) 700–708.

[19] J.J. Jennings Jr, J.H. Zhu, Y. Rbaibi, X. Luo, C.T. Chu, K. Kiselyov, Mitochondrial aberrations in mucolipidosis type IV, J. Biol. Chem. 281 (2006) 39041–39050.
[20] C. Settembre, A. Fraldi, L. Jahreiss, C. Spampanato, C. Venturi, D. Medina, R. Pablo, C. Tacchetti, D.C. Rubinsztein, A. Ballabio, A block of autophagy in lysosomal storage disorders, Hum. Mol. Genet. 17 (2008) 119–129.
[21] C.D. Pacheco, R. Kunkel, A.P. Lieberman, Autophagy in Niemann-Pick C disease is dependent upon beclin-1 and responsive to lipid trafficking defects, Hum. Mol. Genet. 16 (2007) 1495–1503.
[22] J.H. Zhu, F. Guo, J. Shelburne, S. Watkins, C.T. Chu, Localization of phosphorylated ERK/MAP kinases to mitochondria and autophagosomes in Lewy body diseases, Brain Pathol. 13 (2003) 473–481.
[23] P.I. Moreira, S.L. Siedlak, X. Wang, M.S. Santos, C.R. Oliveira, M. Tabaton, A. Nunomura, L.I. Szweda, G. Aliev, M.A. Smith, X. Zhu, G. Perry, Autophagocytosis of mitochondria is prominent in Alzheimer disease, J. Neuropathol. Exp. Neurol. 66 (2007) 525–532.
[24] J.H. Zhu, C. Horbinski, F. Guo, S. Watkins, Y. Uchiyama, C.T. Chu, Regulation of autophagy by extracellular signal-regulated protein kinases during 1-methyl-4-phenylpyridinium-induced cell death, Am. J. Pathol. 170 (2007) 75–86.
[25] A. Yamamoto, L.M. Cremona, J.E. Rothman, Autophagy-mediated clearance of huntingtin aggregates triggered by the insulin-signaling pathway, J. Cell Biol. 172 (2006) 719–731.

Highlighted paper selected by Editor-in-chief

Contribution of Translin to Hematopoietic Regeneration after Sublethal Ionizing Irradiation

Yuko FUKUDA,[a] Reiko ISHIDA,[a] Katsunori AOKI,[b] Kazuhiko NAKAHARA,[c] Tohru TAKASHI,[d] Keiji MOCHIDA,[e] Osamu SUZUKI,[f,1)] Junichiro MATSUDA,[f,1)] and Masataka KASAI*,[a]

[a] *Department of Immunology, National Institute of Infectious Diseases;* [f] *Department of Veterinary Science, National Institute of Infectious Diseases; 1–23–1 Toyama, Shinjuku-ku, Tokyo 162–8640, Japan:* [b] *Department of Hematology, (Internal Medicine), The University of Tokyo; Bunkyo-ku, Tokyo 113–8655, Japan:* [c] *National Institution for Academic Degrees and University Evaluation; 1–29–1 Gakuen-nishimachi, Kodaira, Tokyo 187–8587, Japan:* [d] *New Product Research Laboratories III, Tokyo R&D Center, Daiichi Pharmaceutical Co., Ltd.; 1–16–13 Kitakasai, Edogawa-ku, Tokyo 134–8630, Japan: and* [e] *Bioresource Center, RIKEN; Tsukuba, Ibaraki 305–0074, Japan.*

Received August 29, 2007; accepted November 29, 2007; published online November 29, 2007

The integrity of the genome is threatened by DNA damaging events such as radiation, viral infection and chemicals. Ionizing irradiation is known to cause genotoxic damage through the generation of reactive oxygen species (ROS) and nitrogen species (RNS) and we have found that a signaling pathway for the nuclear translocation of Translin is initiated in association and efficiently blocked by a specific inhibitor of nitric oxide synthase (NOS). This suggests the involvement of inducible nitric oxide synthase (iNOS)-derived nitric oxide (NO) in the nuclear translocation of Translin. To address the functional significance of Translin in the hematopoietic generation system after ionizing irradiation, we generated Translin-deficient (Translin$^{-/-}$) mice and examined hematopoietic colony formation after sublethal ionizing irradiation. We thereby confirmed a severe delay of colony formation in the spleens of Translin$^{-/-}$ as compared with Translin$^{+/+}$ mice. Taken together, the results suggest that Translin contributes to hematopoietic regeneration by acting as a sensor protein for radiation-induced damage.

Key words Translin; ionizing irradiation; hematopoietic regeneration

We have previously shown that expression of the octameric ring protein, Translin, closely parallels the proliferative state in various cell types, with protein synthesis starting in S phase and becoming maximal during the G2/M phase.[2—4)] This pattern of periodic expression is most likely associated with functions in the replication of chromosomal DNA or cell division control. In addition, stable transfectant cells expressing inducible Translin under the control of a tetracycline-responsive promoter incorporate BrdU more efficiently than non-expressing cells. This finding suggests that Translin may participate in process ensuring the replication of DNA as well as the acceleration of cell division. Moreover, confocal microscopic analysis has revealed that Translin is localized at the centrosomes at prophase and the mitotic spindle at metaphase, then shifting to midbodies in late telophase. All of these results suggest that Translin participates in processes ensuring the replication of DNA and cytokinesis in mitotic cell division.

In the present investigation, we generated Translin-deficient mice and addressed the question of whether Translin contributes to hematopoietic regeneration after exposure to ionizing irradiation. Evidence was thereby generated that Translin acts like a sensor protein when cells are exposed to various forms of DNA damage such as ionizing irradiation and oxidative stress.

MATERIALS AND METHODS

Nuclear and Cytosolic Preparations Cells were centrifuged at 1000×***g*** for 5 min and the pellets washed in ice-cold PBS and resuspended in Hypotonic Buffer (10 mM Tris–HCl (pH 7.9), 10 mM KCl, 1.5 mM $MgCl_2$, 0.5 mM PMSF). After homogenization with 20 strokes in a Dounce homogenizer, nuclei were pelleted at 2000×***g*** for 10 min, and the supernatant saved as the cytosolic fraction. Nuclear pellets were washed twice, incubated in Rocking Buffer (20 mM Tris–HCl (pH 7.9), 20% glycerol, 300 mM KCl, 1.5 mM $MgCl_2$, 0.5 mM dithiothreitol (DDT), 0.5 mM phenylmethylsulfonyl fluoride (PMSF)) on ice for 30 min and centrifuged at 13000×***g*** to remove any precipitate. Nuclear and cytosolic preparations were precipitated with 10% trichloroacetic acid (TCA), followed by repeated washing with acetone.

Immunoblotting For detection of Translin, cell pellets were dissolved in sodium dodecyl sulfate (SDS) sample buffer (62.5 mM Tris–HCl (pH 6.8), 2% SDS, 5% glycerol, 0.01% bromophenol blue) and run on 10% acrylamide SDS-polyacrylamide gel electrophoresis (PAGE) under reducing conditions, transferred to Hybond-polyvinylidene difluoride membranes (Amersham Pharmacia Biotech), and probed with affinity-purified rabbit anti-Translin antibody (1 : 500) followed by horseradish peroxidase-conjugated goat anti-rabbit IgG (1 : 1500). Antibody binding was detected by enhanced chemiluminescence according to the manufacturer's instructions (Amersham Pharmacia Biotech).

Generation of Translin-Deficient Mice The coding sequence of the mouse Translin gene encoding the functional protein is composed of six exons. A gene targeting construct was prepared by deleting an entire exon (10.5 kb). The resulting Translin targeting vector, constructed from a strain 129 library (Stratagene) and consisting of a 3.2 kb homology arm derived from the 5′ end of the exon, a PGK-promoter-neo expression cassette, and a 4.0 kb homology arm from the 3′ end of the exon, was linearized with *Eco*RI and introduced into GSI ES cells (derived from 129/SvJ) by electroporation. Surviving colonies after selection were picked and expanded for DNA analysis. Targeted ES cells were injected into the blastocoel cavity of C57/BL6 embryos using a Piezo-driven mi-

* To whom correspondence should be addressed. e-mail: masataka@nih.go.jp

cromanipulator (PrimeTech, Tsuchiura, Japan) to generate chimeric mice which were then bred with C57BL/6 females to obtain heterozygous Translin$^{+/-}$ mutants. These in turn were interbred and found to produce homozygous Translin$^{-/-}$ mice at the expected Mendelian frequency.

Exposure to Ionizing Irradiation K562 cells were exposed to 20-Gy dose of irradiation using a ^{137}Cs source, and then Translin levels in both nuclear and cytoplasmic fractions were examined by Western immunoblot anaysis. To ask whether Translin contributes to hematopoietic regeneration after ionizing irradiation, Translin$^{+/+}$ and Translin$^{-/-}$ mice (8—10 weeks) were exposed to a 4-Gy dose of irradiation. At the indicated times, the histological features of hematopoietic regeneration in the spleen were assessed by hematoxylin and eosin staining.

RESULTS

Translin Expression Level Is Linked to Cell-Cycle Checkpoint Control in Hematopoietic Cells One of the most widely used models for hematopoietic differentiation is that featuring PMA (phorbol 12-myristate 13-acetate) treatment of the pluripotent K562 human leukemia cell line.[5] This results in irreversible cell cycle arrest and induction of megakaryocytic differentiation *in vitro*. To determine whether a link between Translin expression and cell proliferation also exists for the hematopoietic system, K562 cells were treated with PMA and the expression levels of Translin protein at various stages were determined by immunoblotting experiments. After exposure to PMA, in accord with cell cycle arrest, the expression levels of Translin protein gradually decreased (Fig. 1A). Since previous studies showed that megakaryotic differentiation of K562 cells by PMA is induced through the MAPK kinase (MEK)/MAPK pathway,[6] we employed a selective inhibitor of the MEK/MAPK pathway, PD98059,[7] and established that the PMA-induced inhibition of Translin expression was indeed abrogated (Fig. 1B). A similar result was also obtained with NGF-induced inhibition of Translin expression in PC12 cells (data not shown).

Ionizing Irradiation and Oxidative Stress Induce Nuclear Translocation of Translin We previously showed that DNA-damaging reagents, mitomycin C and etoposide initiate a signaling pathway for the nuclear translocation of Translin.[8] To test whether Translin is involved in early responses to irradiation, we examined levels in K562 cells within several hours after irradiation. As expected, the majority of Translin was found in the cytoplasm, but a significant amount was also observed in the nucleus after the exposure (Fig. 2A). Nuclear Translin levels reached a peak at around 6 h and then returned to the basal levels within 24 h. Although the tumor suppressor gene product p53 also increased in response to ionizing irradiation, nuclear levels continued

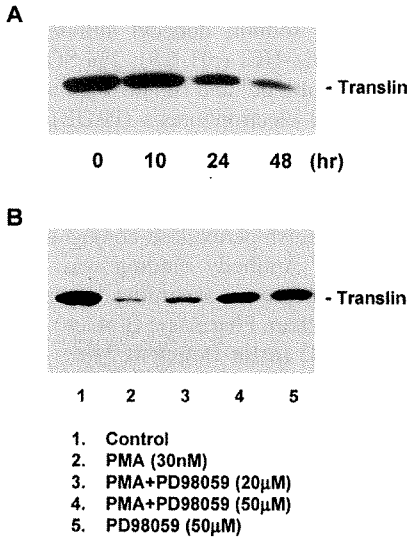

Fig. 1. Expression of Translin Is Linked to Cell-Cycle Checkpoint Control in Hematopoietic Cells

(A) After K562 cells were treated with 10 nM PMA, total cell lysates were assessed at the indicated times for Translin levels by immunoblotting. (B) K562 cells were treated with 30 nM PMA for 48 h and total cell lysates were assessed for Translin levels by immunoblotting. The cells were pretreated with PD98059 (20, 50 μM) for 30 min before addition of PMA.

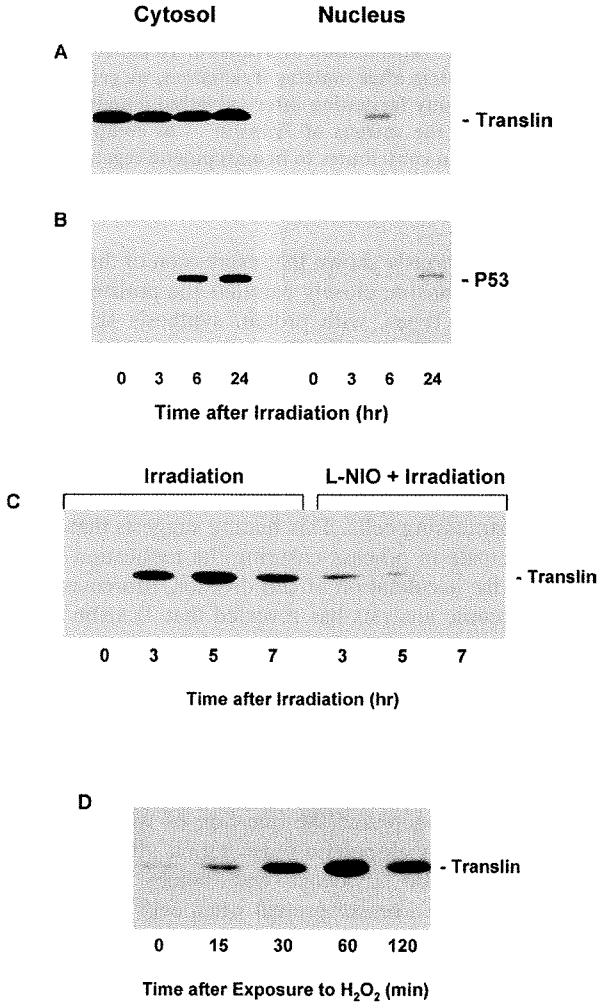

Fig. 2. Ionizing Irradiation and Oxidative Stress Induces Nuclear Transport of Translin

(A) K562 cells were exposed to a 20-Gy dose of irradiation, and then Translin levels in both nuclear and cytoplasmic fractions were assessed at the indicated times. (B) As a control, the same samples in (A) were tested for levels of p53. (C) K562 cells pretreated with L-NIO (50 μM) for 15 min were exposed to a 20-Gy dose of irradiation, and then the nuclear Translin levels were assessed at the indicated times by immunoblotting. (D) K562 cells were pretreated with 10 mM H_2O_2 for 15 min at 37 °C, washed with PBS, further incubated, and assessed at the indicated times for nuclear Translin levels by immunoblotting analysis.

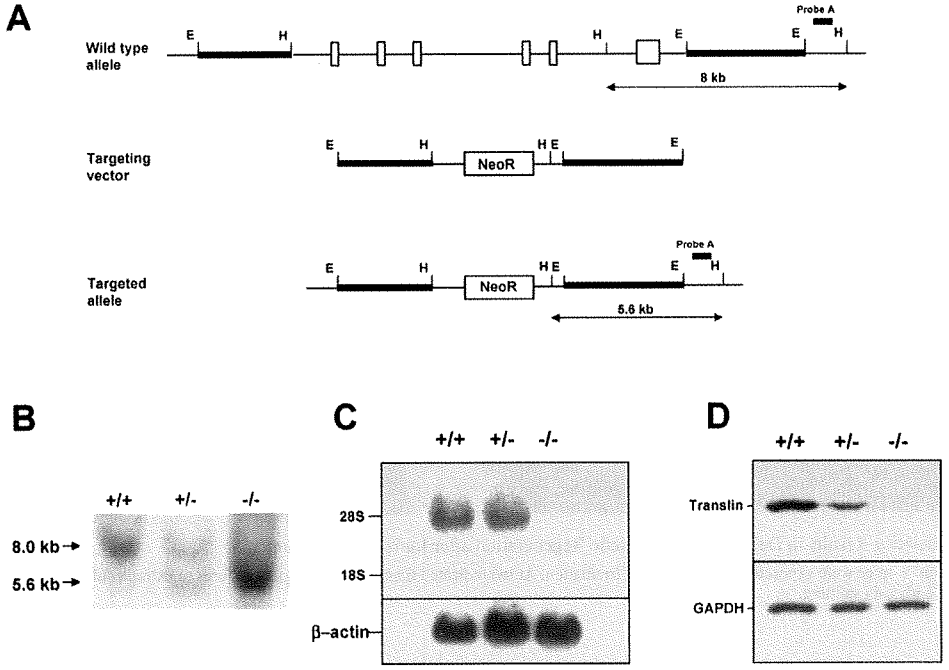

Fig. 3. Generation of Translin$^{-/-}$ Mice

(A) Inactivation of the Translin gene by homologous recombination. The figure shows a restriction map of the mouse Translin gene, the targeting vector, and the structure of the mutated locus following homologous recombination. The coding exons are depicted by boxes. Restriction enzyme abbreviations: E, *Eco*RI; H, *Hin*dIII; NeoR, neomycin resistance. (B) Southern blot analysis of genomic DNA from genotyped embryonic tails. DNA derived from progeny of a Translin$^{+/-}$ cross was digested with *Hin*dIII and hybridized with probe A. The wildtype genomic fragment is 8 kb in size, while the targeted gene is 5.6 kb. Genotypes are indicated above each lane. (C) Northern blot analysis showing absence of Translin transcripts in Translin$^{-/-}$ mice. Total RNA was prepared from testes of wild-type and heterozygous and homozygous mutant mice. Northern blots were probed with a coding region probe, targeting the 3.4-kb Translin transcript. A probe for β-actin was used as a control for sample loading. (D) Western immunoblot analysis showing lack of Translin expression in Translin$^{-/-}$ mice. Total protein was prepared from testes of wild-type and heterozygous and homozygous mutant mice. Protein samples were run on 10% acrylamide SDS-PAGE under reducing conditions, transferred onto a PVDF membrane, and probed using anti-Translin antibodies.

to rise after the Translin levels returned to normal (Fig. 2B).

It was shown recently that exposure to ionizing irradiation results in the activation of inducible nitric oxide synthase (iNOS), which generates nitric oxide (NO), a natural mediator involved in a variety of biological processes, including immune responses, neurotransmission, and vasorelaxation.[9] Overproduction of NOS has been shown to cause DNA damage and trigger repair processes.[10] To ascertain whether NO might be responsible for the nuclear translocation of Translin induced by ionizing radiation, we examined the influence of *N*-iminoethyl-L-ornithine (L-NIO), a specific inhibitor of iNOS.[11] As shown in Fig. 2C, L-NIO reduced the nuclear Translin levels in K562 cells, suggesting the involvement of iNOS-derived NO in the nuclear translocation of Translin during acute radiation responses.

Ionizing irradiation is also known to cause oxidative damage to macromolecules such as proteins, membrane lipids and DNA through the generation of reactive oxygen species (ROS), including H_2O_2, hydroxyl radicals and superoxide.[12,13] H_2O_2 itself is thought to cause DNA breaks and base modifications through generation of hydroxyl radicals. We therefore tested whether oxidative stress due to H_2O_2 could induce nuclear translocation of Translin. Surprisingly, the nuclear Translin levels in K562 cells started to increase within 30 min and reached a peak at around 1 to 2 h after the cells were exposed to H_2O_2, much faster than with ionizing irradiation (Fig. 2D).

Generation of Translin-Deficient Mice To address the functional significance of Translin in the hematopoietic system, we generated mice homozygous for an inactivating mutation of the whole Translin gene. As with its human counterpart, the coding sequence of the mouse Translin gene is assembled from six exons that are spread over a genomic distance of 10.5 kb (Fig. 3A). We prepared a gene targeting construct by deleting entire exons and replacing them with a cassette expressing the neo gene, and the targeted ES clone was then injected into blastocysts to generate chimeric mice. The Translin$^{+/-}$ mice were interbred and found to produce homozygous Translin$^{-/-}$ mice at the expected Mendelian frequency. We confirmed that the wild-type allele is an 8 kb fragment, while the targeted allele is a 5.6 kb fragment by Southern blot hybridization (Fig. 3B). Northern blot analysis demonstrated Translin transcripts to be absent in homozygous mutants (Fig. 3C) and this was confirmed by Western immunoblotting using anti-Translin polyclonal antibodies (Fig. 3D). Translin$^{-/-}$ mice were found to be viable and to have no obvious behavioral abnormalities, while being significantly smaller than their wild-type littermate controls (data not shown).

Translin Contributes to Hematopoietic Regeneration after Ionizing Irradiation In response to ionizing radiation or other environmental stresses, eukaryotic cells are thought to activate signal transduction pathways to arrest cells at specific checkpoints in the cell cycle, to allow repair of damaged DNA.[10] To address the functional significance of Translin in the hematopoietic generation system with reference to acute radiation-responses, we examined hematopoietic colony formation in Translin$^{-/-}$ mice after exposure to

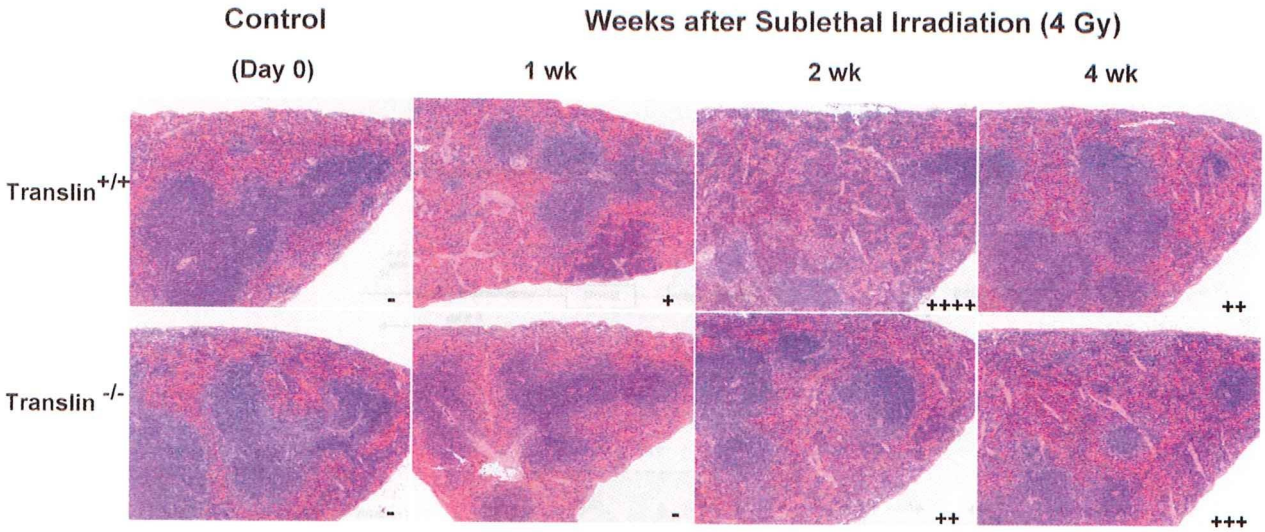

Fig. 4. Translin Deficiency Results in Delayed Hematopoietic Regeneration after Ionizing Irradiation

Translin$^{+/+}$ and Translin$^{-/-}$ mice were exposed to a 4-Gy dose of irradiation. At the indicated times, the histological features of extramedullary hematopoiesis in the spleen were assessed by hematoxylin and eosin staining.

a 4-Gy dose of ionizing irradiation. After 1, 2 and 4 weeks of irradiation, the histological features of extramedullary hematopoiesis in the spleen of Translin$^{+/+}$ and Translin$^{-/-}$ mice were assessed by hematoxylin and eosin staining. The results illustrated in Fig. 4 clearly indicate that the hematopoietic colony formation in the spleen of wild mice started 1 week after irradiation and peaked at 2 weeks. However, the same hematopoietic colony formation in the spleens of Translin$^{-/-}$ mice was delayed more than 2 weeks compared with Translin$^{+/+}$ mice.

DISCUSSION

We have demonstrated that PMA treatment of K562 cells induced inhibition of Translin expression in accord with cell cycle arrest. Moreover, a selective inhibitor of MEK/MAPK pathway, PD98059, abrogated the PMA-induced inhibition of Translin expression. Given the involvement of the MEK/MAPK pathway in growth arrest with concomitant induction of p21$^{WAF1/CIP1}$, a potent inhibitor of cyclin-dependent kinase (CDK) activity,[14] it is conceivable that Translin gene expression is down-regulated by cell cycle arrest, accompanied by induction of CDK inhibitory proteins.

In a previous report,[4] we showed that expression of Translin is associated with cell cycle checkpoint defects in lymphoid cells from cases of Ataxia-telangiectasia (AT), a recessive human genetic disorder resulting from mutations of the Atm gene,[15] characterized by progressive neuro-degeneration, immunologic defects, cancer predisposition, and hypersensitivity to ionizing irradiation.[16,17] While DNA damage responses after ionizing irradiation normally cause cell cycle arrest to allow cells to carry out DNA repair, AT cells show an irradiation-induced cell cycle checkpoint defect.[18] In our data, cell cycle checkpoint defects of AT cells are associated with altered expression of the Translin protein, providing further support for a general tight link with cell proliferation in acute radiation responses.[4] In addition, we found that the nuclear translocation of Translin is induced by ionizing irradiation and efficiently blocked by a specific inhibitor of iNOS. This suggests the involvement of iNOS-derived NO in the nuclear translocation of Translin during acute radiation responses.

The free radical generator H_2O_2 has been found to induce tyrosine phosphorylation of intracellular proteins.[19—21] In this regard, recent studies have demonstrated that H_2O_2 promotes tyrosine phosphorylation and rapid nuclear translocation of STAT3.[22] We found that the nuclear Translin levels reached a peak at around 1 to 2 h after the cells were exposed to H_2O_2, much faster than with ionizing irradiation. While the precise molecular mechanism remains unclear, it may be speculated that exogenously added high dose of H_2O_2 (10 mM) could induce rapid nuclear translocation of Translin by phosphorylation.

To address the functional significance of Translin in the hematopoietic generation system after ionizing irradiation, we generated Translin-deficient mice and examined hematopoietic colony formation after sublethal ionizing irradiation. We confirmed a severe delay of colony formation in the spleens of Translin$^{-/-}$ compared with Translin$^{+/+}$ mice, clearly indicating that Translin contributes the hematopoietic colony formation for radiation-induced damage. Although a number of potential molecules linked with stress responses and altered cell cycle regulation have been identified,[23] we have shown that Translin is involved in the mechanism by which hematopoietic cells regenerate after exposure to ionizing irradiation. Thus, the present results point to opportunities for translating research findings into clinical application in the recovery from radiation-induced injury.

Acknowledgment This work was supported by the Budget for Nuclear Research of the MEXT, awarded to M.K.

REFERENCES

1) Present Address: *Laboratory of Experimental Animal Models, National Institute of Biomedical Innovation; 7–6–8 Saito-Asagi, Ibaraki,*

Osaka 567–0085, Japan.

2) Aoki K., Suzuki K., Sugano T., Tasaka T., Nakahara K., Kuge O., Omori A., Kasai M., *Nature Genetics*, **10**, 167—174 (1995).
3) Aoki K., Ishida R., Kasai M., *FEBS Lett.*, **443**, 363—366 (1999).
4) Ishida R., Aoki K., Kasai M., *FEBS Lett.*, **525**, 105—110 (2002).
5) Sutherland J. A., Turner A. R., Mannoni P., McGann L. E., Turc J. M., *Biol. Response Mod.*, **5**, 250—262 (1986).
6) Herrera R., Hubbell S., Decker S., Petruzzelli L., *Exp. Cell Res.*, **238**, 407—414 (1998).
7) Dudley D., Pang L., Decker S., Bridges A., Saltiel A., *Proc. Natl. Acad. Sci. U.S.A.*, **92**, 7686—7689 (1995).
8) Kasai M., Matsuzaki T., Katayanagi K., Omori A., Maziarz R. T., Strominger J. L., Aoki K., Suzuki K., *J. Biol. Chem.*, **272**, 11402—11407 (1997).
9) Nurse P., *Cell*, **91**, 865—867 (1997).
10) Weinert T., *Cell*, **94**, 555—558 (1998).
11) Nathan C., *Cell*, **82**, 873—876 (1995).
12) Schwarz M. A., Lazo J. S., Yalowich J. C., Allen W. P., Whitmore M., Bergonia H. A., Tzeng E., Billiar T. R., Robbins P. D., Lancaster J. R., Jr., *et al.*, *Proc. Natl. Acad. Sci. U.S.A.*, **92**, 4452—4456 (1995).
13) McCall T., Feelisch M., Palmer R., Moncada S., *Br. J. Pharmacol.*, **102**, 234—238 (1991).
14) Pumiglia K. M., Decker S. J., *Proc. Natl. Acad. Sci. U.S.A.*, **94**, 448—452 (1997).
15) Savitsky K., Bar-Shira A., Gilad S., Rotman G., Ziv Y., Vanagaite L., Tagle D. A., Smith S., Uziel T., Sfez S., *Science*, **268**, 1749—1753 (1995).
16) Swift M., Morrell D., Massey R., Chase C., *N. Engl. J. Med.*, **325**, 1831—1836 (1991).
17) Thacker J., *Int. J. Radiat. Biol.*, **66**, S87—S96 (1994).
18) Lavin M. F., Shiloh Y., *Annu. Rev. Immunol.*, **15**, 177—202 (1997).
19) Schieven G. L., Kirihara J. M., Burg D. L., Geahlen R. L., Ledbetter J. A., *J. Biol. Chem.*, **268**, 16688—16692 (1993).
20) Schieven G. L., Mittler R. S., Nadler S. G., Kirihara J. M., Bolen J. B., Kanner S. B., Ledbetter J. A., *J. Biol. Chem.*, **269**, 20718—20726 (1994).
21) Nakamura K., Hori T., Sato N., Sugie K., Kawakami T., Yodoi J., *Oncogene*, **8**, 3133—3139 (1993).
22) Carballo M., Conde M., El Bekay R., Martín-Nieto J., Camacho M. J., Monteseirín J., Conde J., Bedoya F. J., Sobrino F., *J. Biol. Chem.*, **274**, 17580—17586 (1999).
23) Bakkenist C. J., Kastan M. B., *Cell*, **118**, 9—17 (2004).

Chemical Chaperone Therapy: Clinical Effect in Murine G_{M1}-Gangliosidosis

Yoshiyuki Suzuki, MD,[1] Satoshi Ichinomiya, MS,[1] Mieko Kurosawa, PhD,[2] Masato Ohkubo, MD,[2] Hiroshi Watanabe, MD,[3] Hiroyuki Iwasaki, MD,[3] Junichiro Matsuda, PhD,[4] Yoko Noguchi, AS,[4] Kazuhiro Takimoto, PhD,[5] Masayuki Itoh, MD,[6] Miho Tabe, BS,[7] Masami Iida, PhD,[8] Takatoshi Kubo, MS,[8] Seiichiro Ogawa, PhD,[9] Eiji Nanba, MD,[10] Katsumi Higaki, PhD,[10] Kousaku Ohno, MD,[11] and Roscoe O. Brady, MD[12]

Certain low-molecular-weight substrate analogs act both as in vitro competitive inhibitors of lysosomal hydrolases and as intracellular enhancers (chemical chaperones) by stabilization of mutant proteins. In this study, we performed oral administration of a chaperone compound *N*-octyl-4-epi-β-valienamine to G_{M1}-gangliosidosis model mice expressing R201C mutant human β-galactosidase. A newly developed neurological scoring system was used for clinical assessment. *N*-Octyl-4-epi-β-valienamine was delivered rapidly to the brain, increased β-galactosidase activity, decreased ganglioside G_{M1}, and prevented neurological deterioration within a few months. No adverse effect was observed during this experiment. *N*-Octyl-4-epi-β-valienamine will be useful for chemical chaperone therapy of human G_{M1}-gangliosidosis.

Ann Neurol 2007;62:671–675

G_{M1}-gangliosidosis (OMIM 230500) is a hereditary human disorder with progressive central nervous system damage, visceromegaly, and skeletal dysplasias in children and adults, caused by mutations of the gene *GLB1* (3p21.33) coding for lysosomal β-galactosidase (EC 3.2.1.23) that catalyzes hydrolysis of ganglioside G_{M1} and related compounds.[1]

In 2003, we proposed chemical chaperone therapy for brain pathology in G_{M1}-gangliosidosis.[2] The first original studies in this direction had been published on mutant α-galactosidase A in Fabry's disease, using galactose[3] and 1-deoxygalactonojirimycin.[4] We then found *N*-octyl-4-epi-β-valienamine (NOEV) as a potent stabilizer of mutant β-galactosidase activity in G_{M1}-gangliosidosis.[2] It increased mutant β-galactosidase activity in cultured fibroblasts from more than 30% of patients.[5]

On the other hand, we developed a novel method to assess neurological alterations in G_{M1}-gangliosidosis model mice by modifying neurological tests in human infants and young children.[6] This technique was applied to monitor their clinical course under chaperone treatment. We found that NOEV prevents neurological deterioration in this animal model.

Materials and Methods

G_{M1}-Gangliosidosis Model Mice

We maintained a C57BL/6-based congenic knock-out (KO) mouse strain with β-galactosidase deficiency[7] and a transgenic (Tg) mouse strain overexpressing R201C mutant human β-galactosidase.[2] Care of experimental animals was performed in accordance with the Guidelines on Animal Experimentation of International University of Health and Welfare (Otawara, Japan). Wild-type (WT) mice (C57BL/6Cr) were purchased from Japan SLC (Shizuoka, Japan).

Neurological Assessment

Quantitative neurological assessment consisted of 11 test items.[6] Each item was scored in four grades (0–3) based on increasing severity of abnormality. The total scores were periodically followed. Reliability and reproducibility of this test method have been established.[6]

N-Octyl-4-epi-β-valienamine Administration and Determination

Tg or WT mice were provided 1mM aqueous solution of NOEV hydrochloride ad libitum. The average daily intake of NOEV was 75μg/gm (75mg/kg) body weight. The NOEV concentration was determined by combined liquid chroma-

From the [1]Graduate School, [2]Center for Medical Science, and [3]Clinical Research Center, International University of Health and Welfare, Otawara; [4]Biological Resource Division, National Institute of Biomedical Innovation, Ibaraki City, Osaka; [5]Division of Experimental Animal Research, National Institute of Infectious Diseases, Shinjuku-ku, Tokyo; [6]Department of Mental Retardation and Birth Defect Research, National Institute of Neuroscience, National Center of Neurology and Psychiatry, Kodaira, Tokyo; [7]Biochemistry Section, Analysis Center for Medical Science, SRL Inc, Hachioji; [8]Central Research Laboratories, Seikagaku Corporation, Higashi-Yamato, Tokyo; [9]Department of Biosciences and Informatics, Faculty of Science and Technology, Keio University, Kohoku-ku, Yokohama; [10]Division of Functional Genomics, Research Center for Bioscience and Technology, Tottori University; [11]Division of Child Neurology, Tottori University Faculty of Medicine, Yonago, Japan; and [12]Developmental and Metabolic Neurology Branch, National Institute of Neurological Disorders and Stroke, National Institutes of Health, Bethesda, MD.

Received Jul 25, 2007, and in revised form Sep 18. Accepted for publication Sep 28, 2007.

Current address for Dr Watanabe, Division of Neuronal Network, Institute of Medical Science, The University of Tokyo, Tokyo 108-8639, Japan.

Current address for Dr Iwasaki, National Rehabilitation Center for Disabled Children, Tokyo 173-0037, Japan.

This article includes supplementary material available via the Internet at http://www.interscience.wiley.com/jpages/0364-5134/suppmat

Published online Nov 9, 2007, in Wiley InterScience (www.interscience.wiley.com). DOI: 10.1002/ana.21284

Address correspondence to Dr Suzuki, International University of Health and Welfare Graduate School, Room L-423, 2600-1 Kita-Kanemaru, Otawara 324-8501, Japan. E-mail: suzukiy@iuhw.ac.jp

tography and tandem mass spectrometry system (Fig 1). For neurological assessment, 16 Tg mice were given NOEV from 2 months of age, and they were compared clinically with the other 16 Tg mice without NOEV treatment.

General Pathology, Neuropathology, and Quantitative Immunohistochemistry

The mice were perfused through the heart with 4% phosphate-buffered paraformaldehyde, and tissues were used for pathology and immunohistochemistry.[2,8] We further performed immunohistochemical quantitation of ganglioside G_{M1} in the brain by confocal fluorometry (Fig 2).

Enzyme Assay

β-Galactosidase and α-galactosidase A were assayed with 4-methylumbelliferyl derivatives (Nacalai Tesque, Kyoto) as substrates[9] and galactosylceramidase with 6-hexadecanoylamino-4-methylumbelliferyl β-galactoside (Erasmus MC, Rotterdam, the Netherlands).[10] Protein was determined with Micro TP-Test Wako (Wako Pure Chemical Industries, Osaka, Japan).

Blood Chemistry and Urinalysis

Blood was collected by cardiac puncture and centrifuged. Plasma was analyzed using FUJI DRI-CHEM 3000V (Fuji Film, Tokyo, Japan) for 14 test items, including glutamic-oxalacetic transaminase, glutamic-pyruvic transaminase, and others, as indicated by this analysis kit. Urine was performed by collection by external pressure or direct puncture of the bladder, using Uro-Labstix SG-L (Bayer Medical, Tokyo, Japan).

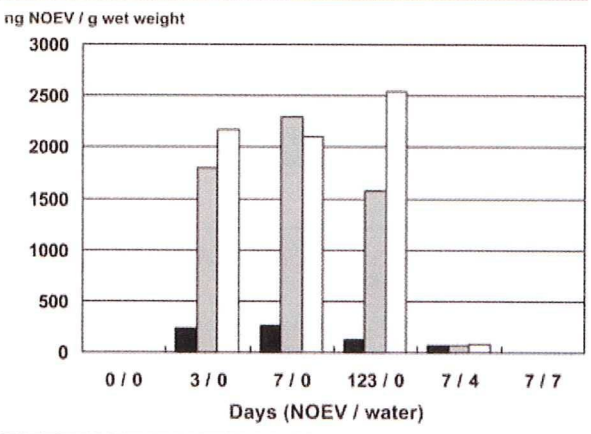

Fig 1. N-*Octyl-4-epi-β-valienamine (NOEV) concentrations in mouse tissues.* Black bars *indicate brain;* gray bars *indicate liver;* white bars *indicate kidney. Tissue content is measured in ng/gm wet weight. 0/0: water only (n = 2); 3/0: NOEV for 3 days (n = 2); 7/0: NOEV for 7 days (n = 2); 123/0: NOEV for 123 days (n = 1); 7/4: NOEV for 7 days, followed by water for 4 days (n = 2); 7/7: NOEV for 7 days, followed by water for 7 days (n = 2).*

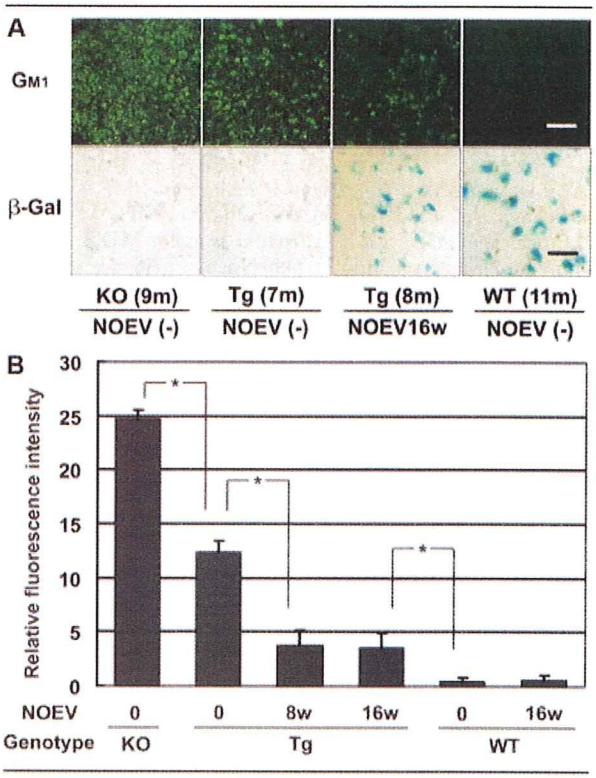

Fig 2. Immunohistochemical analysis of the R201C mouse brain. (A) Histochemical stain of G_{M1} and β-galactosidase. (B) Quantitative confocal immunohistochemistry of G_{M1}. Each column *indicates the mean of relative fluorescence intensity in the mouse brain* (vertical bar = *standard error of the mean).* $^{*}p < 0.05$. *KO (0w) = KO mouse; water only (n = 2; age: 7 and 9 months). Tg (0w) = Tg mouse; water only (n = 3; age = 7, 11, and 15 months). Tg (8w) = Tg mouse;* N-*octyl-4-epi-β-valienamine (NOEV) for 8 weeks (n = 2; age = 10 and 11 months). Tg (16w) = Tg mouse; NOEV for 16 weeks (n = 1; age = 9 months). WT (0w) = WT mouse; water only (n = 1; age = 11 weeks). WT (16w) = WT mouse; NOEV for 16 weeks (n = 1; age = 9 months). KO = knock-out; Tg = transgenic; WT = wild type. See supplementary material for additional methodology details.*

Results

N-Octyl-4-epi-β-valienamine Concentration in Mouse Tissues

The NOEV concentration increased in the brain, liver, and kidney of WT mice within 3 days immediately after starting treatment, remained at the same level for as long as 123 days of continuous administration, decreased rapidly within 4 days after discontinuation of treatment, and completely disappeared within 7 days (see Fig 1). The concentration was almost the same in the liver and kidney, and about 10% to 15% in the brain compared with the two extraneural tissues. Tissue concentrations remained the same after 8 to 16 weeks of NOEV administration in Tg mice (data not shown).

Pathology and Immunohistochemistry

There were no specific changes in the liver, spleen, kidney, lung, heart, thymus, pancreas, or skeletal muscle of NOEV-treated mice. Bleeding, hemostasis, leukocyte infiltration, or cytoplasmic vacuolation was observed in some sporadic WT, Tg, or KO mice with or without treatment (data not shown). Immunohistochemical stain showed a marked decrease in G_{M1} storage and increase in the enzyme activity in almost all areas of the brain after 8 to 16 weeks of NOEV treatment (see Fig 2A). This observation was confirmed quantitatively by confocal fluorometry, indicating a significant decrease of G_{M1} in the NOEV-treated Tg mouse brain (see Fig 2B).

Enzyme Activities

β-Galactosidase activity increased remarkably during NOEV treatment for 8 to 16 weeks in Tg mice, particularly in the liver and spleen (data not shown). In the brain, the enzyme activity in Tg mice reached 30% to 40% of that in WT mice. Galactosylceramidase and α-galactosidase A activities did not change in this experiment.

Neurological Assessment

We first compared the three genotypes without NOEV treatment (Fig 3A). The total score remained low (<5) in the WT mouse until 24 months. It was high (almost 10) in the KO mouse already at 5 months (middle symptomatic stage), and increased to 25 at 9 to 10 months (late stage). The Tg mouse showed slower progression than the KO mouse. However, even at 2 to 4 months (early symptomatic stage), the mean of total score was significantly greater than that of the WT mouse.

NOEV treatment was started at 2 months of age (see Fig 3B). There was no significant difference for the first 2 months between the two groups with or without treatment. Then a definite statistical difference was detected at 5 to 7 months of age, although the score increased gradually also in the treatment group. This clinical benefit was not evident when the treatment was started at 5 months over the ensuing 5 months (data not shown).

Blood Chemistry and Urinalysis

Glutamic-oxalacetic transaminase and glutamic-pyruvic transaminase were high in some WT, Tg, or KO mice examined. However, they were not related to the genotype, clinical course, age, or NOEV treatment. Urinalysis was normal in all mice examined.

Discussion

In this study, we investigated the clinical effect of the chemical chaperone NOEV after our first report on laboratory data in G_{M1}-gangliosidosis mouse model.[2]

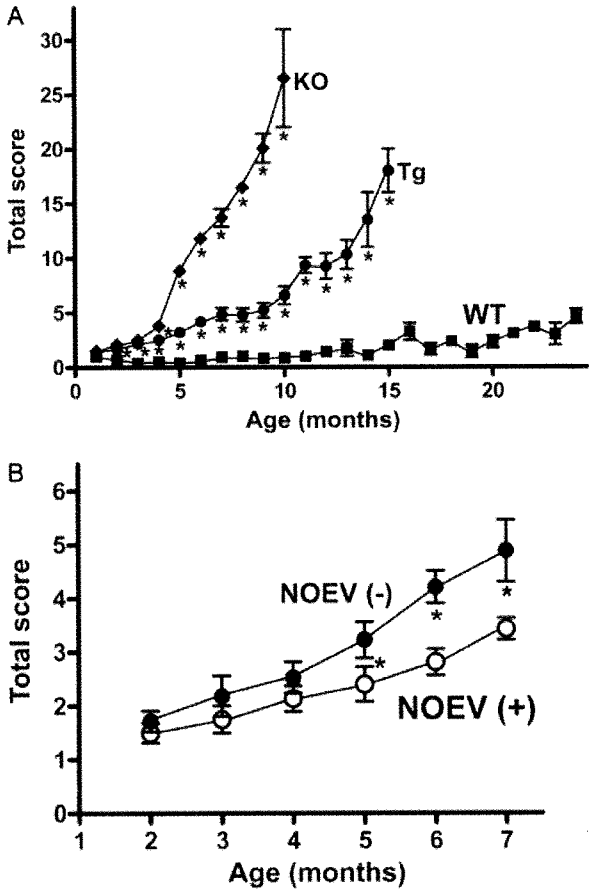

Fig 3. Neurological assessment scores in G_{M1}-gangliosidosis mouse model. (A) Clinical course in three mouse genotypes without N*-octyl-4-epi-β-valienamine (NOEV) treatment. The quantitative neurological assessment consisted of the following 11 test items: gait, posture/forelimb, posture/hind limb, posture/trunk, posture/tail, avoidance response, rolling over, body righting acting on head, parachute reflex, horizontal wire netting (stepping through interstice), and vertical wire netting (clinging and holding body).*[6] *The mice were scored in four grades based on increasing severity of abnormality for each test item: 0 (normal), 1 (slightly abnormal), 2 (moderately abnormal), and 3 (severely abnormal). The highest score was 33 for those with the most extensive neurological abnormalities. We used GraphPad Prism 4 (GraphPad Software, San Diego, CA) for unpaired Student's* t *test.* Black squares *indicate wild-type (WT) mouse;* black circles *indicate transgenic (Tg) mouse;* black diamonds *indicate knock-out (KO) mouse.* Vertical bars *indicate standard error of the mean (SEM).* $^*p < 0.05$ *(WT vs Tg, and Tg vs KO).* $n = 10, 10, 11, 24, 28, 17, 21, 13, 2$ *for KO (2–10 months);* $n = 32, 11, 19, 18, 29, 17, 17, 18, 18, 17, 11, 6, 4, 2$ *for Tg (2–15 months);* $n = 11, 5, 12, 12, 9, 18, 21, 21, 16, 19, 18, 8, 10, 9, 11, 9, 8, 9, 9, 10, 7, 2, 3$ *for WT (2–24 months). (B) Clinical effect of NOEV therapy in Tg mice. The experimental conditions were the same as Figure 3A.* Black circles *indicate Tg mouse, nontreated;* white circles *indicate Tg mouse, treated with NOEV.* Vertical bars *indicate SEM.* $^*p < 0.05$. $n = 16$ *for both treated and nontreated mice.*

NOEV is an epimer of *N*-octyl-β-valienamine,[11,12] a potent inhibitor of β-galactosidase in vitro[13,14] and a potent inducer to express mutant β-galactosidase activity in human and murine fibroblasts and tissues.[2] NOEV was effective in almost all patients with juvenile G_{M1}-gangliosidosis and in some with infantile G_{M1}-gangliosidosis.[5] Most patients were compound heterozygotes. We expect a successful therapeutic effect if one of the mutant genes is responsive to NOEV. The efficacy of enhancement varied among different mutations. Eight human mutant enzymes responded positively to NOEV, including known common mutations (K. Higaki and colleagues, unpublished data). The optimal NOEV concentration was 0.2μM for R457Q and 2μM for R201C and R201H.[5] We estimate that NOEV therapy will be successful in at least one-third of patients with G_{M1}-gangliosidosis.

This study indicates that orally administered NOEV entered the central nervous system from the bloodstream across the blood–brain barrier. The compound did not accumulate in the tissues examined during oral administration for 4 months. The increase of β-galactosidase activity and reduction of G_{M1} reflected changes of NOEV concentration in mouse tissues. We did not analyze urinary oligosaccharides.

In this study, we tried two new approaches for quantitative evaluation of the NOEV effect in murine G_{M1}-gangliosidosis: immunohistochemistry and clinical assessment. Quantitative confocal fluorometry demonstrated a remarkable decrease of G_{M1} in the mouse brain after NOEV treatment. The neurological assessment scores corresponded well with laboratory data.

Early chaperone therapy resulted in a positive clinical effect within a few months, although complete arrest or prevention of disease progression was not achieved under the current experimental conditions. The latency before the clinical effect was longer if the therapy was started in the late symptomatic stage. We conclude that early treatment at the early stage of disease is mandatory for prevention of brain damage. We do not know the optimal dose of NOEV at present in murine G_{M1}-gangliosidosis.

No significant adverse effect was observed during NOEV administration up to 6 months. Random increases of plasma glutamic-oxalacetic transaminase and glutamic-pyruvic transaminase concentrations were not related to genotype or NOEV treatment. Blood collection by direct cardiac puncture after ethyl ether anesthesia and thoracotomy may have partly contributed to abnormal release of intracellular enzymes into the extracellular fluid. We did not observe excessive enzyme enhancement in the course of NOEV treatment, but it may cause some metabolic derangement in human and mouse tissues.

So far we demonstrated effectiveness of chemical chaperone therapy in G_{M1}-ganglosidosis,[2,5] Gaucher's disease,[15,16] and Fabry's disease.[4] A short-term effect was reported on a Fabry's disease patient with galactose,[17] and other investigators confirmed the effectiveness of chaperone therapy in Gaucher's disease fibroblasts.[18] In addition, the effect of chaperone treatment has been reported in G_{M2}-gangliosidosis[19] and Pompe's disease.[20] Theoretically, this principle can be applied to other lysosomal diseases, if a specific chaperone compound becomes available for each target enzyme. Furthermore, other neurogenetic diseases may be considered for chemical chaperone therapy. We expect that studies in this direction will open a new aspect of molecular therapy for inherited metabolic diseases with central nervous system involvement in the near future.

This research was supported by the Ministry of Education, Culture, Science, Sports, and Technology of Japan (13680918, 14207106, 16300141) and the Ministry of Health, Labour and Welfare of Japan (H10-No-006, H14-Kokoro-017, H17-Kokoro-019) (all grants to Y.S.).

References

1. Suzuki Y, Nanba E, Matsuda J, Oshima A. β-Galactosidase deficiency (β-galactosidosis): G_{M1}-gangliosidosis and Morquio B disease. In: Scriver CR, Beauder AL, Sly WS, et al., eds. The online metabolic and molecular bases of inherited disease. New York: McGraw-Hill, 2006. Available at: http://genetics.accessmedicine.com.
2. Matsuda J, Suzuki O, Oshima A, et al. Chemical chaperone therapy for brain pathology in G_{M1}-gangliosidosis. Proc Natl Acad Sci USA 2003;100:15912–15917.
3. Okumiya T, Ishii S, Takenaka T, et al. Galactose stabilizes various missense mutants of α-galactosidase in Fabry disease. Biochem Biophys Res Commun 1995;214:1219–1224.
4. Fan J, Ishii S, Asano N, Suzuki Y. Accelerated transport and maturation of lysosomal α-galactosidase A in Fabry lymphoblasts by an enzyme inhibitor. Nat Med 1999;5:112–115.
5. Iwasaki H, Watanabe H, Iida M, et al. Fibroblast screening for chaperone therapy in β-galactosidosis. Brain Dev 2006;28:482–486.
6. Ichinomiya S, Watanabe H, Maruyama K, et al. Neurological assessment of G_{M1}-gangliosidosis model mice. Brain Dev 2006;29:210–216.
7. Matsuda J, Suzuki O, Oshima A, et al. β-Galactosidase-deficient mouse as an animal model for G_{M1}-gangliosidosis. Glycoconj J 1997;14:729–736.
8. Itoh M, Matsuda J, Suzuki O, et al. Development of lysosomal storage in mice with targeted disruption of the β-galactosidase gene: a model of human G_{M1}-gangliosidosis. Brain Dev 2001;23:379–384.
9. Sakuraba H, Aoyagi T, Suzuki Y. Galactosialidosis (β-galactosidase neuraminidase deficiency): a possible role of serine thiol proteases in the degradation of β-galactosidase molecules. Clin Chim Acta 1982;125:275–282.
10. Wiederschain G, Raghavan S, Kolodny E. Characterization of 6-hexadecanoylamino-4-methylumbelliferyl-β-D-galactopyranoside as fluorogenic substrate of galactocerebrosidase for the diagnosis of Krabbe disease. Clin Chim Acta 1992;205:87–96.
11. Ogawa S, Ashiura M, Uchida C, et al. Synthesis of potent β-D-glucocerebrosidase inhibitors: N-alkyl-β-valienamines. Bioorg Med Chem Lett 1996;6:929–932.

12. Ogawa S, Kobayashi E, Kabayama K, et al. Chemical modification of β-glucocerebrosidase inhibitor N-octyl-β-valienamine: synthesis and biological evaluation of N-alkanoyl and N-alkyl derivatives. Bioorg Med Chem 1998;6:1955–1962.
13. Ogawa S, Kobayashi-Matsunaga Y, Suzuki Y. Chemical modification of the β-glucocerebrosidase inhibitor N-octyl-β-valienamine: Synthesis and biological evaluation of 4-epimeric and 4-O-(β-D-galactopyranosyl) derivatives. Bioorg Med Chem 2002;10:1967–1972.
14. Ogawa S, Sakata Y, Ito N, et al. Convenient synthesis and evaluation of glycosidase inhibitory activity of α- and β-galactose-type valienamines, and some N-alkyl derivatives. Bioorg Med Chem 2004;12:995–1002.
15. Lin H, Sugimoto Y, Ohsaki Y, et al. N-Octyl-β-valienamine up-regulates activity of F213I mutant β-glucosidase in cultured cells: a potential chemical chaperone therapy for Gaucher disease. Biochim Biophys Acta 2004;1689:219–228.
16. Lei K, Ninomiya H, Suzuki M, et al. Enzyme enhancement activity of N-octyl-β-valienamine on β-glucosidase mutants associated with Gaucher disease. Biochim Biophys Acta 2007; 1772:587–596.
17. Frustaci A, Chimenti C, Ricci R, et al. Improvement in cardiac function in the cardiac variant of Fabry's disease with galactose-infusion therapy. N Engl J Med 2001;345:25–32.
18. Sawkar A, Cheng W, Beutler E, et al. Chemical chaperones increase the cellular activity of N370S β-glucosidase: a therapeutic strategy for Gaucher disease. Proc Natl Acad Sci USA 2002;99:15428–15433.
19. Tropak M, Reid S, Guiral M, et al. Pharmacological enhancement of β-hexosaminidase activity in fibroblasts from adult Tay-Sachs and Sandhoff patients. J Biol Chem 2004;279: 13478–13487.
20. Parenti G, Zuppaldi A, Gabriela P, et al. Pharmacological enhancement of mutated α-glucosidase activity in fibroblasts from patients with Pompe disease. Mol Ther 2007;15:508–514.

ELSEVIER

Brain & Development 29 (2007) 210–216

BRAIN & DEVELOPMENT
Official Journal of the Japanese Society of Child Neurology

www.elsevier.com/locate/braindev

Original article

Motor and reflex testing in G_{M1}-gangliosidosis model mice

Satoshi Ichinomiya [a,d], Hiroshi Watanabe [b], Kimiko Maruyama [a], Hiroko Toda [a], Hiroyuki Iwasaki [b], Mieko Kurosawa [c], Junichiro Matsuda [e], Yoshiyuki Suzuki [a,*]

[a] *Graduate School, International University of Health and Welfare, Otawara, Japan*
[b] *Clinical Research Center, International University of Health and Welfare, Otawara, Japan*
[c] *Center for Medical Science, International University of Health and Welfare, Otawara, Japan*
[d] *Department of Rehabilitation, Otawara Red Cross Hospital, Otawara, Japan*
[e] *Biological Resource Division, National Institute of Biomedical Innovation, Ibaraki City, Japan*

Received 21 June 2006; received in revised form 2 August 2006; accepted 20 August 2006

Abstract

A large number of genetic disease model mice have been produced by genetic engineering. However, phenotypic analysis is not sufficient, particularly for brain dysfunction in neurogenetic diseases. We tried to develop a new assessment system mainly for motor and reflex functions in G_{M1}-gangliosidosis model mice. Two genetically engineered model mouse strains were used for this study: the β-galactosidase-deficient knockout mouse representing infantile G_{M1}-gangliosidosis (severe form), and transgenic mouse representing juvenile G_{M1}-gangliosidosis (mild form). We modified human child neurology techniques, and selected eleven tests for motor assessment and reflex testing. The test results were scored in four grades: 0 (normal), 1 (slightly abnormal), 2 (moderately abnormal), and 3 (severely abnormal). Both disease model mouse strains showed high scores even at the apparently pre-symptomatic stage of the disease, particularly with abnormal tail and hind limb postures. Individual and total test scores were well correlated with the progression of the disease. This method is simple, quick, and reproducible. The testing is sensitive enough to detect early neurological abnormalities, and will be useful for monitoring the natural clinical course and effect of therapeutic experiments in various neurogenetic disease model mice, such as chemical chaperone therapy for G_{M1}-gangliosidosis model mice.

Keywords: G_{M1}-gangliosidosis; Genetic engineering; Disease model mouse; Motor assessment; Reflex testing; Mouse neurology

1. Introduction

The recent advance of molecular technology has made it possible to produce a large number of disease model animals, particularly genetically engineered mice. Many of them present with progressive or non-progressive central nervous system manifestations of various severities. At present the neurological status is assessed mainly by gross clinical observations or with sophisticated instruments mainly for evaluation of cortical functions, such as memory, learning, and behavior. The past clinical experience taught us that clinical impression was not always supported by neuropathologic or neurochemical analysis, particularly for rapidly progressive neurological diseases. Sometimes brain pathology was far more severe or extensive than expected by clinically recognizable minimal cerebral dysfunction. Accordingly the neurological course has not been well delineated in many neurogenetic diseases in the mouse species.

For more than 15 years we performed molecular analyses of β-galactosidase deficiency disorders (β-galactosidosis) [1]: cDNA cloning [2], mutation analyses [3,4],

* Corresponding author. Tel./fax: +81 287 24 3229.
E-mail address: SuzukiY@iuhw.ac.jp (Y. Suzuki).

0387-7604/$ - see front matter © 2006 Elsevier B.V. All rights reserved.
doi:10.1016/j.braindev.2006.08.014